

JIMMA UNIVERSITY

SCHOOL OF GRADUATE STUDIES

JIMMA INSTITUTE OF TECHNOLOGY

FACULTY OF CIVIL AND ENVIROMENTAL ENGINEERING

STRUCTURAL ENGINEERING STREAM

MODELING AND ANALYSIS OF PRE-CAST CONCRETE BEAM BASED ON

UNIFIED THEORY OF CONCRETE

Msc Thesis

A Thesis Submitted to the School of Graduate Study of Jimma University in Partial Fulfillment
of the Requirements for the Degree of Masters of Science in Structural Engineering

By

ASHAGRE FETENE

AUGUST, 2020
JIMMA, ETHIOPIA

JIMMA UNIVERSITY
SCHOOL OF GRADUATE STUDIES
JIMMA INSTITUTE OF TECHNOLOGY
FACULTY OF CIVIL AND ENVIROMENTAL ENGINEERING
STRUCTURAL ENGINEERING STREAM

MODELING AND ANALYSIS OF PRE-CAST CONCRETE BEAM BASED ON
UNIFIED THEORY OF CONCRETE

A Thesis Submitted to the School of Graduate Study of Jimma University in Partial Fulfillment
of the Requirements for the Degree of Masters of Science in Structural Engineering.

By

ASHAGRE FETENE

ADVISOR: Engr. ELMER.C.AGON (ASS.PROF.)

CO-ADVISOR: Engr. EDEN SHUKRI

AUGUST, 2020

JIMMA, ETHIOPIA

JIMMA UNIVERSITY

SCHOOL OF GRADUATE STUDIES

JIMMA INSTITUTE OF TECHNOLOGY






FACULTY OF CIVIL AND ENVIRONMENTAL ENGINEERING

STRUCTURAL ENGINEERING CHAIR

MODELING AND ANALYSIS OF PRECAST CONCRETE BEAM BASED ON UNIFIED THEORY OF CONCRETE

ASHAGERE FETENE

APPROVED BY BOARD OF EXAMINERS

- | | | |
|------------------------------------|---|-----------------------|
| 1. Engr. Elmer C. Agon, Asso. Prof |  | <u>08 / 09 / 2020</u> |
| Main advisor | Signature | Date |
| 2. Engr. Eden Shukri, MSc |  | <u>10 / 09 / 2020</u> |
| Co-advisor | Signature | Date |
| 3. Dr. Binaya Patnaik |  | <u>04 / 09 / 2020</u> |
| External Examiner | Signature | Date |
| 4. Engr. Vinoth Raj Kumar |  | <u>04 / 09 / 2020</u> |
| Internal Examiner | Signature | Date |
| 5. Engr. Abinet Alemseged |  | <u>10 / 09 / 2020</u> |
| Chairperson | Signature | Date |

DECLARATION

I, the undersigned, declare that the thesis is my original work, and has not been presented for a degree in any other university and that all secondary sources referred to in this work have been duly acknowledged.

Name: Ashagre Fetene


Signature: _____

Place: Jimma University
Jimma Institute of Technology
Jimma

Date: August, 2020

Engr. Elmer C.Agon (Asso.Prof.)

Advisor

 08 / 09 / 2020

Signature

Date

Engr. Eden Shukri (M.Sc.)

Co-Advisor

10/ 09/ 2020

Signature

Date

ACKNOWLEDGEMENT

I owe a special debt of gratitude to my advisors Engr. Elemer C. Agon (Ass.Prof.) and Eng. Eden Shukri for their support, guidance and valuable comment to bring this work for this stage. I would like to extend my heartfelt gratitude to Engr. Elemer C. Agon once more for his patience, understanding, persistence, and assistance beyond the research work. His confidence in me has being very inspiring, his concern and support in personal matter. Whether or not he conscious of this fact, I have learned a great deal from him. I wish to sincerely thank Mr. Kefyalehu Zerfu, Abinet Alemseged, and Nigatu Solomon for yours concern about my study and yours willingness to help me in manipulation of ABAQUS software. My special acknowledgement also goes to all my Institute who have always been supporting and encouraging me throughout my stay.

I would like to extend my thanks to Jimma University, Jimma Institute of Technology and for the financial support and JIT structural Chair senior staffs for their valuable advises.

Finally, I wish to express my gratitude to my beloved family, who unsparingly encouraging and supporting me in angles during all these years.

Above all, thanks to the almighty God for being with me and helping me in all ups and downs; without His will, nothing could have happened.

ABSTRACT

A reinforced concrete structure may be subjected to four basic types of actions: bending, axial load, shear and torsion. All of these actions can, for the analyzed and designed by a single unified theory based on the three fundamental principles of mechanics of materials: namely, the stress equilibrium condition, the strain compatibility condition, and the constitutive laws of concrete and steel. Because the compatibility condition is taken into account, this theory can be used to reliably predict the strength of a structure, as well as its load–deformation behavior. Concrete and steel bar are idealized as uniform and continuity materials, smeared (average) stress-strain relations of concrete and steel bars should be used. The smeared stress-strain relationships of concrete for precast concrete beam have been proposed in soften compression curve and stiffening tensile curve. This study proposes a smeared stress-strain relationship of steel bars embedded in concrete. Also a Belarbi’s model is proposed, the analytical approaches are stated. Using the smeared stress-strain relationship of concrete and steel bars for model of precast beam.

In this study, the pre-cast concrete beam has been modelled and analyzed when subjected to two point loads at one third spans from each support, using Finite Element Analysis tool, popularly called ABAQUS software. The modelled and analyzed precast beam cross-section having size 120mm×80mm with 2 numbers of 12 mm diameter bars as bottom reinforcement, 12mm diameter bars as top reinforcement and 6 mm diameter at 150 mm c/c as shear reinforcement. The behaviour of the analyzed precast beam has been observed in terms of the flexural cracking, crack pattern, failure load, bucking failure of the stirrups, and maximum deflection. Based on the analysis carried out on the pre-cast beams using ABAQUS Software, it is found that results are more sensitive to mesh size, compressive strength, dilation angle, viscosity parameter, and static load. The model is validated using different experiment results for pre-cast beam elements presented in the literature. Comparison is made between the experimental results and finite element analyses with respect to initial crack formation and the ultimate load capacity of pre-cast beams. The results indicate a good agreement with load vs. deflection curve and observed crack patterns.

Key words: *Finite element simulation, Modelling, Pre-cast concrete beam, Unified theory, flexural cracking*

TABLE OF CONTENT

DECLARATION	I
ACKNOWLEDGEMENT	II
<i>ABSTRACT</i>	III
TABLE OF CONTENT	IV
LIST OF FIGURES	VII
LIST OF TABLES	IX
ACRONYMS	X
CHAPTER ONE	1
INTRODUCTION	1
1.1. Background of the Study	1
1.2. Statement of the problem.....	2
1.3. Objectives of the Study.....	3
1.3.1. General Objective.....	3
1.3.2. Specific Objectives.....	3
1.4. Significance of the study.....	3
1.5. Scope and Limitation of the Study.....	3
CHAPTER TWO	5
REVIEW OF RELATED LITERATURE	5
2.1. Unified Theory of Concrete Structures.....	5
2.1.1. Softened Truss Model for Membrane Elements	6
2.1.2. Softened stress–strain relationship of concrete in compression.....	9
2.1.3. Steel bars Embedded in Concrete and Smearred Stress-Strain Curves	10
2.2. Modeling and Analysis of pre-cast concrete beam	11
2.3. Concrete Damage Plasticity Model	12
2.3.1. Uniaxial tension and compression stress behavior.....	13
2.4. Description of Experimental Test	14
CHAPTER THREE	16
RESEARCH METHODOLOGY	16
3.1. Analysis and Modeling of Pre-cast Beam.....	16

3.1.1. Description of Reference Tests specimen for validation Kebede M. (2009)	16
3.1.2. Descriptions of Specimen.....	17
3.1.3. Nonlinear constitutive behavior of concrete and steel bars analysis using unified theory of concrete	18
3.2. Study Variables	23
3.2.1. Dependent variables	23
3.2.2. Independent variables	23
3.3. Finite element modeling	24
3.3.1. Geometric modeling.....	24
3.3.2. Concrete elements	24
3.3.3. Compressive behavior	26
3.3.4. Tension Stiffening Relationship.....	27
3.3.5. Reinforcement bar	28
3.3.6. Loading and Boundary Condition.....	29
3.3.7. Finite Element Mesh	29
CHAPTER FOUR.....	31
RESULT AND DISCUSSION	31
4.1. Numerical Analysis of pre-cast beam based on unified theory	31
4.1.1. Smearred tensile stress-strain Curve of concrete in tension.....	31
4.1.2. Softened stress-strain curves of concrete in compression.....	33
4.1.3. Steel bars embedded in Concrete and Smearred Stress-Strain Curves.....	34
4.1.4. Belarbi's Model for Smearred Stress-Strain Curve of Mild steel.....	37
4.1.5. Bilinear Model for Smearred Stress-Strain Curve	38
4.2. Modeling and Analysis of Precast Beam	42
4.2.1. Analysis of Pre-cast Concrete Block.....	43
4.2.2. Prediction of the Buckling Resistance of Stirrups	48
4.2.3. Load Combinations	51
4.2.4. Deflection requirement for Service Load.....	52
4.3. Finite Element Analysis Method	53
4.3.1. Numerical Simulations	53
4.3.2. Validation of Finite Element Model.....	57

CHAPTER FIVE	64
CONCLUSION AND RECOMMENDATIONS	64
5.1. CONCLUSION.....	64
5.2. RECOMMENDATIONS.....	65
REFERENCE	66
APPENDIXES	68

LIST OF FIGURES

Figure 2.1: Stress condition in reinforced concrete membrane element.....	7
Figure 2.2: Stress and strain between two cracks	10
Figure 2.3: Space truss model of precast beam and slab block arrangements	11
Figure 2.4: Response of concrete to uniaxial loading in (a) Tension; (b) Compression	13
Figure 2.5: Two Point Loading.....	14
Figure 2.6: Photo of Test Specimens: (a) Photo of Bending Test setup and Specimens; (b). Photo of Buckled Stirrups (Kebede M, 2009)	15
Figure 3.1: Specimen of pre-cast Concrete beams: (a) For Group-I; (b) For Group-II; and (c) precast beam cross-section 1-1.	18
Figure 3.2: Terms for Compressive Stress-Strain Relationship /Definition of inelastic strain (Abaqus Manual, 2014)	26
Figure 3.3: Terms for Tension Stiffening Model (Abaqus Manual, 2014).....	28
Figure 3.4: Loading and Boundary condition of Model	29
Figure 3.5: Finite Element Mesh	30
Figure 3.6: Geometric assembly of Pre-cast concrete Beam	30
Figure 4.1: Smearred tensile stress-strain relation of concrete: (a) for grade C-25 concrete, (b) for grade C-30 concrete, (c) for grade C-20 concrete	32
Figure 4.2: Compressive Stress-Strain curve of concrete: (a) for grade C-25 concrete,(b) for grade C-30 concrete, (c) for grade C-20 concrete	34
Figure 4.3: Pre-cast concrete beams: (a) longitudinal Pre-cast Beam section; (b) Beam section	35
Figure 4.4: Smearred stress-strain curves of mild steel	37
Figure 4.5: Smearred Stress-Strain Curve of mild steel for percentage of steel (ρ) and cracking strength of concrete (f_{cr}) as parameter.	40
Figure 4.6: Model for Analysis and Design.....	43
Figure 4.7: Stress and strain Profile for pre-cast concrete block	43
Figure 4.8: Moment capacity of upper part of the pre-cast beam.....	48
Figure 4.9: Numerical result for FEA model of Bucked stirrups: (a) For reinforcement of stirrup of 6mm diameter, (b) For reinforcement of stirrup of 8mm diameter.....	50
Figure 4.10: General details of the FEA model	53

Figure 4.11: Load-deflection response observed experimentally and numerically with respect to meshing size: (a) Precast Beam, PCB-2, (b) Precast Beam PCB-6..... 55

Figure 4.12: Effect of concrete dilation angle 56

Figure 4.13: Effect of viscosity parameter, μ 57

Figure 4.14: Numerical result for FEA modeling of beam PCB-2; (a) contour lines of compression stresses along precast beam span; (b) tensile damage of along precast beam span; (c) contour line steel stress distribution. 58

Figure 4.15: Numerical results for FEA modeling of beam PCB-4: (a) contour lines of tensile stresses along beam span; (b) contour lines of tensile stresses at bottom reinforcement bar; (c) compression damage of along precast beam span..... 59

Figure 4.16: Flexural cracking 60

Figure 4.17: Load – Deflection response observed experimentally and numerically with respect to meshing size for Pre-cast beam, PCB-2 61

Figure 4.18: Load – Deflection response observed experimentally and numerically with respect to meshing size for Pre-cast beam, PCB-4 62

Figure 4.19: load-deflection behavior for different value of f_{ck} (a) PCB-2, (b).PCB-6..... 63

LIST OF TABLES

Table 1: Details of specimen.....	17
Table 2: summary of the plasticity parameters used for the CDP model	25
Table 3: Pre-cast beam dimensions and materials of steel	35
Table 4: Pre-cast beams and reinforcement quantities	36
Table 5: Martial Property for Concrete.....	36
Table 6: Summarized Material Property for the pre-cast beams	36
Table 7: Summarized Material Property for the pre-cast beams	36
Table 8: Summarized Materials Property by Bilinear Model.....	39
Table 9: Summarized Materials Property by Bilinear Model for different crack strength.....	39
Table 10: Selected of Smeared Stress and Smeared Strain of Mild steel from three model for grade C-25 concrete.....	41
Table 11: Selected of Smeared Stress and Smeared Strain of Mild steel from three model for grade C-30 concrete.....	41
Table 12: Selected of Smeared Stress and Smeared Strain of Mild steel from three model for grade C-20 concrete.....	41
Table 13: Values of “ ΔM ” and “ Cs ” (KEBEDE, 2009).....	46
Table 14: Buckling resistance of different sizes of bar.....	47
Table 15: Moment capacity of the upper part of the precast beam.....	49
Table 16: Deflection of Pre-cast concrete Beam at concrete pouring stage	52
Table 17: Comparison between FEA results and Experimental	57
Table 18: Comparison FEA and Experimental result.....	60

ACRONYMS

A_s	Area of tensile reinforcement bars
α	Angle of principal concrete stress (d-axis)
f_y^*	Apparent yield stress
P	applied load
f_{ck}	Characteristic of concrete compressive strength
ε_t^{ck}	Cracking strain of concrete
ε_{cr}	Cracking concrete of strain
ε_t^{ck}	Cracking strain
f_{cr}	Cracking tensile strength
f_{cr}	Cracking strength of concrete
d'	Concrete cover to the center of the reinforcement bars
CPDM	Concrete Plastic Damage Model
C_c	Compressive force in the concrete
ε_{oc}^{el}	Compression elastic strain of undamaged material
C_c	Compression force for concrete
M_{Comp}	Compression Moment
CFT	Compression field theory
DPM	Damage plasticity model
H	Depth of pre-cast block
a	Depth of the stress block
C	Depth to the neutral axis
ψ	Dilation angle
d	effective depth for be pre-cast concrete block
FEA	Finite Element Analysis
FEAP	Finite Element Programs
FA-STM	Fixed –angle softened truss model
h_s	Height of PCB above the pre-cast block
HCB	Hollow concrete block
E_o	Initial modulus of elasticity

ε_c^{in}	Inelastic strains
τ_s	Longitudinal shear force in the legs of the stirrups
ε_{cu}	Maximum compressive strain in the concrete
E_c	Modulus of elasticity of concrete
E_{cm}	Modulus of elasticity of the concrete
E_s	Modulus of elasticity of mild steel bars
M	Model (experimental) moment
MCFT	Modified Compression field theory
C	Neutral axis depth of the pre-cast block from the top fiber
γ_c, γ_s	Partial safety factors for concrete and steel, responsibility
PCB	Precast Concrete Beam
PCB	Pre-cast beam
ε_t^{pl}	Plastic strain
$\varepsilon:$	Plastic potential eccentricity
ρ_l	Reinforcement ratio in the l-direction
ρ_t	Reinforcement ratio in the t-direction
K_c	Ratio of the second stress invariant
ρ	Reinforcement ratio,
RC	Reinforced concrete
RA-STM	Rotating –angle softened truss model
V_c	Section capacity of shear force
V_s	Shear resistance of stirrups
P_{shear}	Shear force of precast beam
σ_d	Smearred principal compressive stress
σ_r	Smearred principal tensile stress
f_l	Smearred stress of steel bars in l-direction
f_t	Smearred stress of steel bars in t-direction
ε_d	Smearred (average) principal compressive d-direction
ε_r	Smearred (average) principal tensile r-direction
σ_t	Smearred tensile stress
f_{cm}	Smearred (or average) compressive strength of the concrete

ε_s	Strain in mild steel bars
f_s	Stress in mild steel bar
ε_s	Strain in the steel reinforcement
f_s	Stress in mild steel bars
SMM	Softened membrane model
f_{ctm}	Tensile strength of concrete
d_t	Tensile damage parameter values of concrete
ε_{ot}^{el}	Tensile Elastic strain of undamaged material
$P_{tensile}$	Tension force of precast beam
T_s	Tensile force in the reinforcement bars
2D	Two dimension element
3D	Three dimension element
ε_t	Total tensile strain
M_u	Ultimate moment
ε_{cu}	Ultimate strain
γ_{HCB}	Unit weight of hollow concrete blocks
ε_y	Yield strain in mild steel
f_y	Yield stress in mild steel bars

CHAPTER ONE

INTRODUCTION

1.1. Background of the Study

In general precast concrete structures competitive in variety of residential, commercial, industrial, transportation and many other types of structures. Precast concrete structures, assembled from high-quality plant produced products, provide superior flexibility for achieving the required degree of fire resistance, sound control, energy efficiency and durability. The availability of a variety of materials and finishes makes it possible to render virtually any desired aesthetic character. Furthermore, the construction speed possible with precast concrete minimizes on-site labor costs, reduces the cost of interim financing, and thus provides important overall economic structure.

Unified theory of concrete structures develops an integrated theory that encompasses the various stress states experienced by reinforced concrete structures under the various loading conditions of bending, axial load, shear and torsion. Upon synthesis, the new rational theories replace the many empirical formulas currently used. The unified theory is divided in to six model components: (a). the struts-and –ties model; (b) the equilibrium (plasticity) truss model; (c).The Bernoulli compatibility truss model; (d) the Mohr compatibility truss model, (e) the softened truss model; and (f) the softened membrane model. Hsu presents the six models as rational tools for the solution of the basic types of stress, focusing on the significance of their intrinsic consistencies and their inter-relationships. Because of its inherent rationality, this unified theory of reinforced concrete can serve as the basis for the formulation of a universal and international design code (Thomas T.C, 2010)

Pre-cast concrete beam is widely used in Ethiopia. Pre-cast beam is rectangular in cross section. Production and transportation of the hollow concrete block for the ribbed slab and the form work still are costly and need improvements. That is why efforts are made to model cross section pre-cast beam in this study. The rectangular cross-section of precast beam carries bending, axial load, shear and torsion. The magnitudes of axial load, bending, shear and torsion action are obtained by unified theory concrete in this study. The analysis can be based on either linear or nonlinear material laws, and the cross-sections can either be uncracked or cracked. The precast reinforced concrete structures have received considerable attention in recent years. An element isolated from such a structure is subjected to membrane stress. Since understanding of the behavior of a reinforced concrete element is the key to the

analysis of the whole structure, a softened truss model theory has been developed for the nonlinear analysis of such membrane elements (Hsu, 1993). The softened truss model incorporates the three fundamental principles of the mechanics of materials: stress equilibrium, strain compatibility and constitutive laws of materials. An accurate prediction by the softened truss model depends strongly on the constitutive laws of the concrete and steel in the elements. In this study the material models taken by softened truss model approach were presented. The smeared stress- strain relationship for reinforcement bars are calculated using Belarbi model closer to the actual condition.

With the continuous development of finite element theory and computer technology, the development of finite element analysis software is maturing. ABAQUS, as one of the largest universal finite element analysis software, is increasingly commonly used in research works and engineering. Because not only does it have high speed, high accuracy and low cost analysis of numerical calculation of finite element analysis software, but also has a more user-friendly operator interface and visualization results, especially when it is used in the nonlinear analysis of reinforced concrete structure. Steel and concrete frictional contact in the embedded technology by ABAQUS is reinforced concrete elements will be embedded in the unit to achieve. The constitutive model is based on a smeared crack approach, i.e. smeared (or average) stresses and smeared (or average) strains are used in this study.

The concrete damaged plasticity model assumes that the two main failure mechanisms in concrete are the tensile cracking and the compressive crushing. In this model, the uniaxial tensile and compressive behaviour is characterized by damaged plasticity. Using the concrete damage plasticity model to investigate the behavior and failure mechanism.

In this study non-linear constitutive behavior of the concrete and the steel bars is analyzed using unified theory of concrete in Microsoft excel. Pre-cast concrete beam is modeled and analyzed by applying static load considering concrete strength, steel yield strength, modeling simply-supported pre-cast concrete beam with equal depths, different span length, longitudinal reinforcement, and stirrups as a parameter and validated with experimental study conducted by Kebede in 2009.

1.2. Statement of the problem

The low cost member of Pre-cast concrete beam have been design based on linear theory of concrete and bare bars steel bars, this approach has demerits on predicting the resistance of

pre-cast concrete beam when the concrete and the steel bar behave non-linearly for checking serviceability. The constitutive principles of both concrete and steel are not considered which has a greater effect on crack and deflection control.

1.3. Objectives of the Study

1.3.1. General Objective

The general objective of this study was to model and analyze of Pre-cast concrete beam using Finite element software called ABAQUS 6.14.

1.3.2. Specific Objectives

- To assess smeared tensile stress-strain relation of concrete pre-cast beam using the different material types
- To study smeared tensile stress-strain relation of steel precast beam using different methods, and compare the result from standards.
- To create a finite element model of the pre-cast concrete beam using ABAQUS Version 14, and compare results of this model under static loading with the experimentally data obtained from the low cost member of pre-cast concrete beam (Kebede M.,2009)
- To analyze the load-deflection response at mid-span and maximum deflection of the pre-cast concrete beam using ABAQUS.

1.4. Significance of the study

The unified theory concrete appreciation to all their graduate/undergraduate students, who contributed greatly to the development of the unified theory. The finite element method is an advanced and well-known method which has become an important tool and is increasingly used by practicing engineers. It makes it possible to take an account in nonlinear response.

1.5. Scope and Limitation of the Study

The main part of this study deals with the modeling and analysis of response of pre-cast concrete beam subjected to static load using finite element analysis. The most typical reinforcement bar size and span length of the precast concrete beam is considered in this study.

The finite element methods important to study the behaviour of concrete members with geometry, material properties, reinforcement amount and load combination which became an important tools practical engineers it makes possible to take an into account non-linear response. Material property, support condition and loading condition that used in the experiment used for validation were applied in the finite model of this study. Load-displacement response, buckling of stirrups and failure model were parameters used to validate. The loads were applied in the pre-cast beam according to the experimental study used for validation. After checking the finite element model reflects the real world result, the parametric study and sensitivity analysis were carried out by considering five parameters that are concrete strength, steel yield strength, precast beam span length , and precast beam section.

CHAPTER TWO

REVIEW OF RELATED LITERATURE

2.1. Unified Theory of Concrete Structures

Unified Theory of Concrete Structures, the integrated the action of four major forces (axial load, bending, shear, torsion), in 1, 2, 3 – dimensions, which culminated into a set of unified theories to analyze and design concrete buildings and infrastructure for maximum safety and economy. the unified theory concrete structure consisted of five component models: (1) the struts-and ties model for design of local regions; (2) the equilibrium (plasticity) truss model for predicting the ultimate strengths of members under all four actions; (3) the Bernoulli compatibility truss model for linear and nonlinear theories of bending and axial load; (4) the Mohr compatibility truss model for the linear theory of shear and torsion; and (5) the softened truss model.

Belarbi and Hsu (1994, 1995) developed the rotating-angle softened truss model (RA-STM). This model made two improvements over the CFT: (1) the tensile stress of concrete was taken into account so that the deformations could be correctly predicted; and (2) the smeared (or average) stress–strain curve of steel bars embedded in concrete was derived on the ‘smeared crack level’ so that it could be correctly used in the equilibrium and compatibility equations which are based on continuous materials. Shortly after the development of the rotating-angle model, Pang and Hsu (1996) and Hsu and Zhang (1997) reported the fixed-angle softened truss model (FA-STM) that is capable of predicting the ‘concrete contribution’ V_c by assuming the cracks to be oriented at the fixed angle, rather than the rotating angle. Zhu, Hsu and Lee (2001) derived a rational shear modulus that is a function of the compressive and the tensile stress–strain curves of concrete. Taking into account the Poisson effect, Hsu and Zhu (2002) developed the softened membrane model (SMM) which could satisfactorily predict the entire monotonic response of the load–deformation curves, including the pre-cracking and the post-cracking responses, as well as the ascending and the descending branches (Hsu and Mo, 2010).

The precast concrete for use as a construction material. The benefits and advantages of using precast concrete building products are limited only by the designer’s imagination and knowledge of how to “engineer” the material. Engineering precast concrete requires unique design considerations not required for most other building materials. When designing precast

concrete, the designer needs to consider manufacturing, handling and erection aspects of product in addition to analysis and design for in-place loads. It is not uncommon for these items to be the controlling factors in the design.

There are two key points that need to be addressed in the application of nonlinear FEA to reinforced concrete (RC) structures: the establishment of nonlinear constitutive models of RC elements and the development of nonlinear finite element methods specifically for reinforced concrete structures. The behavior of reinforced concrete elements should be thoroughly understood before being applied to the finite element method. Many researchers have developed different types of analytical models of reinforced concrete such as truss models, orthotropic models, nonlinear elastic models, plastic models, micro models, etc. The orthotropic model stands out both in accuracy and in efficiency as compared with the other models. Since the 1980s, orthotropic models have been developed to predict the shear behavior of reinforced concrete elements by many researchers: Vecchio and Collins (1981, 1982), Balakrishnan and Murray (1988), Crisfield and Wills (1989), Izumo et al. (1992), Shin et al. (1991), Hsu (1993), Belarbi and Hsu (1995), Pang and Hsu (1995), Sittipunt and Wood (1995), Pang and Hsu (1996), Hsu and Zhang (1997), Ayoub and Fillippou (1998), Kaufmann and Marti (1998), Vecchio (2000, 2001), Ile and Reynouard (2000), Belletti et al. (2001), Hsu and Zhu (2002), Kwon and Spacone (2002), Palermo and Vecchio (2003), Foster et al. (2004), and Mansour and Hsu (2005a, 2005b).

2.1.1. Softened Truss Model for Membrane Elements

A reinforced concrete membrane element is subjected to in-plane shear stresses and normal stresses as shown in Figure 2.1(a). The stresses σ_l , σ_t and τ_{lt} are defined in the $l-t$ coordinate of the longitudinal steel bars. This set of in-plane stresses σ_l , σ_t and τ_{lt} is equivalent to set of principal stresses, σ_2 and σ_1 , acting along the principal 2-1 coordinate system, Figure 2.1(d). The angle between the 2-1 coordinate and the $l-t$ coordinate is called the fixed angle α_2 because this angle remains unchanged when the applied stresses σ_l , σ_t and τ_{lt} increase proportionally. Based on the reinforced concrete sign convention for Mohr's circle, a positive shear stress τ_{lt} is one that causes clockwise rotation of a reinforced concrete element (Hsu, 1993).

The first set of cracks occurs when the principal tensile stress σ_1 reaches the tensile strength of concrete. These diagonal cracks will separate the concrete into a series of concrete struts.

In general, when an element is reinforced with different amounts of steel in the l – and t – directions, the direction of the principal stresses, in concrete after cracking will continuously deviates from the direction of the applied principal stresses, as the applied load increases proportionally. The post-cracking principal stresses in the concrete are defined by the d-r coordinate in Figure 2.1e. The angle α between the d-axis and l –axis continues to rotate away from the initial angle α_2 throughout the loading history. As such, the angle α is called the rotating-angle. The average principal compressive stress and the average principal tensile stress in the concrete are designated σ_d and σ_r , respectively.

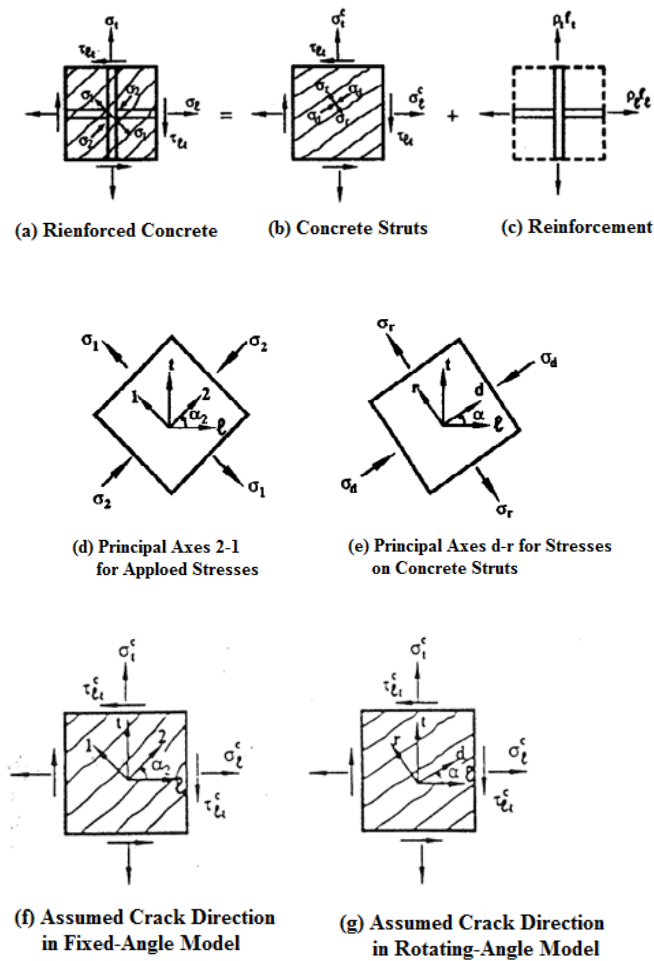


Figure 2.1: Stress condition in reinforced concrete membrane element

2.1.1.1. Equilibrium Equations

The two - dimensional equilibrium condition relates the smeared (average) internal stresses in the concrete (σ_d and σ_r) and in the reinforcement (f_l and f_t) to the applied stresses (σ_l , σ_t and τ_{lt}). Utilizing the transformation of concrete stresses and assuming that the steel bars can resist only axis stresses, the superposition of concrete stresses and steel stresses results in (Hsu, 1993):

$$\sigma_l = \sigma_d \cos^2 \alpha + \sigma_r \sin^2 \alpha + \rho_l f_l \quad \text{Eq. 1}$$

$$\sigma_t = \sigma_d \sin^2 \alpha + \sigma_r \cos^2 \alpha + \rho_t f_t \quad \text{Eq. 2}$$

$$\tau_{lt} = (\sigma_r - \sigma_d) \sin \alpha \cos \alpha \quad \text{Eq. 3}$$

Where σ_d and σ_r are Smeared (average) principal compressive and tensile stresses of cracked concrete, respectively; ρ_l and ρ_t are the percentages of reinforcement in the l and t directions, respectively; f_l and f_t are Smeared (average) stresses of steel bars in l and t directions, respectively and α are Angle of principal concrete stress (d-axis) with respect to longitudinal steel bars (l – axis).

2.1.1.2. Compatibility Equations

The two-dimensional compatibility condition expresses the state of strains within the element. Assuming that the d- and r- are also principal axes for strains, and then the transformation of average strains between the $l - t$ coordinate system ($\varepsilon_l, \varepsilon_t, \gamma_{lt}$) and the d-r principal axes ($\varepsilon_d, \varepsilon_r$) gives:

$$\varepsilon_l = \varepsilon_d \cos^2 \alpha + \varepsilon_r \sin^2 \alpha, \quad \text{Eq. 4}$$

$$\varepsilon_t = \varepsilon_d \sin^2 \alpha + \varepsilon_r \cos^2 \alpha, \quad \text{Eq. 5}$$

$$\gamma_{lt} = 2 (\varepsilon_r - \varepsilon_d) \sin \alpha \cos \alpha, \quad \text{Eq. 6}$$

Where ε_d and ε_r are Smeared (average) principal compressive and tensile strains in the d and r directions, respectively.

2.1.1.3. Constitutive Laws

Based on the principles of mechanics, the stresses in the equilibrium equations need to be related to the strain in the compatibility equations through the constitutive laws of materials. The analysis/ design of the membrane element of Figure 2.1(a) requires four stress-strain relationships, i.e., concrete in compression, concrete in tension and steel in longitudinal directions as follows. In other words the solution of the above six equilibrium and compatibility equations requires three set of constitutive laws: (1). concrete in compression, relating σ_d and ε_d ; (2).concrete in tension, relating σ_r and ε_r , and (3).mild steel relating f_l to ε_l and f_t to ε_t . The three sets of constitutive laws are discussed in the following section:

$$\sigma_d = f_1(\epsilon_d, \epsilon_r) \quad \text{Eq. 7}$$

$$\sigma_r = f_2(\epsilon_r) \quad \text{Eq. 8}$$

$$f_1 = f_3(\epsilon_1) \quad \text{Eq. 9}$$

$$f_t = f_4(\epsilon_t) \quad \text{Eq. 10}$$

Because the equilibrium and compatibility equations are derived for a continuous material, the stress–strain relationships of concrete reinforcement must relate smeared stresses to smeared strains. The derivation of functions f_1 through f_4 in Equation 7 through 10 was the focus of an extensive study carried out at the University of Houston (Belarbi and Hsu, 1994, 1995; Pang and Hsu, 1995; Zhang, 1992, 1995). In this study to improve the mathematical expression for the constitutive laws required in the softened truss model. Based on this study, the following constitutive laws are derived (chapter3).

In this study the material models taken by softened membrane model approach. The smeared stress-strain relationship for reinforcement bars are calculated using Belarbi model closer to the actual condition, and also the smeared stress-strain relationships of concrete and steel were expressed analytically models by Tamaiet.al (1987); the Belarbi and Hsu (1994); Bilinear model.

2.1.2. Softened stress–strain relationship of concrete in compression

The primary characteristic of the constitutive law of concrete in compression is the softening of peak stress in comparison to the companion cylinder. The variables that may affect the softening phenomenon were studied in a systematic manner. These variables include the tensile strain, the tensile stress, the load path and the nature of applied loads (biaxial tension-compression Vs, pure shear), the percentage of steel, the spacing of steel bars, the ratio of reinforcement's bars, and the concrete strength. Among the variables investigated, the severity of cracking expressed in terms of ϵ_c , the concrete strength and to a certain extent the load path were found to be the main variable. The softening coefficient was also found to be inversely proportional to $\sqrt{f_{cm}}$. The graphic representation of the stress-strain relationship of the softened concrete struts is shown in Figure 2.1, is established in the d-r coordinate as follows (Zhang and Hsu, 1998).

2.1.3. Steel bars Embedded in Concrete and Smeared Stress-Strain Curves

When a reinforcing steel bar is embedded inside a concrete, the cracked response of the reinforced concrete becomes stiffer than the reinforcement alone. This phenomenon is called tension-stiffening and represents the ability of cracked concrete to carry tensile stresses. After the formation of cracks in concrete, the strains along a steel bar decrease from a maximum at the crack to a minimum at the midpoint of two adjacent cracks as shown in Figure 2.2. Accordingly, the concrete stresses should be zero at the crack and increase to a maximum value at midpoint between two adjacent cracks, while the bar steel stresses decrease from a maximum value at the crack to a minimum value midway between two cracks. Hence, the smeared (or average) stress-strain relationships of a steel bar embedded in concrete must be obtained by smearing the stresses and strains between two adjacent cracks (Belarbi and Hsu, 1994).

The tensile stresses in concrete between two adjacent cracks are transferred from the reinforcement via bond stresses between the reinforcement and the surrounding concrete. Hence, bond characteristics govern the internal stress distribution in concrete and reinforcement. Crack width and crack spacing can greatly affect localized reinforced concrete behavior. In most cases however, local bond characteristics are only of minor importance to the overall structural behavior as long as they do not induce failure. It is sufficient to take into account the tension-stiffening effect in a smeared sense and to ignore the bond stresses at the local level.

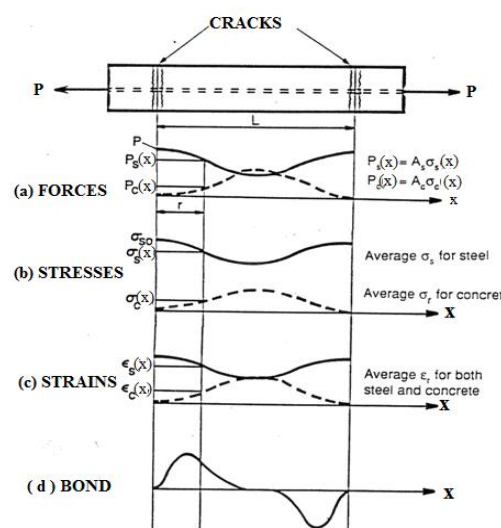


Figure 2.2: Stress and strain between two cracks

Smearred strain of an embedded steel bar is the sum of the strain due to the crack widths and the strain of the intact concrete between cracks. At first yield of the steel, the stress in a steel bar will reach the bare-bar yield stress at the cracks and will become smaller away from the cracks. Hence, the smeared yield stress in the embedded bar will be less than the yield stress of a bare bar. This indicates that the post-yield portion of the smeared stress-strain relationships in the post-yielding region of reinforcement eluded the attention of researchers until 1994, when Belarbi and Hsu (1994) proposed a new smeared stress-strain curve for mild steel bars. In this bilinear model the smeared stress-strain curve of embedded steel bars in concrete before yielding is the same as the linear stress-strain curve of bare steel bar. After yielding however, the smeared stress-strain relationship of embedded steel bars in concrete is a sloping straight line below that of bare bars

In this study the material models taken by softened membrane model approach. The smeared stress-strain relationship for reinforcement bars are calculated using Belarbi model closer to the actual condition ,and also the smeared stress-strain relationships of concrete and steel were expressed analytically models by Tamaiet.al (1987); the Belarbi and Hsu (1994); Bilinear model

2.2. Modeling and Analysis of pre-cast concrete beam

The pre-cast beams must provide adequate strength during all phases of construction. The unit is most critical when the self-weight of the wet insitu concrete is added to the self-weight of the pre-cast plank and the slab hollow concrete block as shown in Figure 2.3 (MH, 2005).

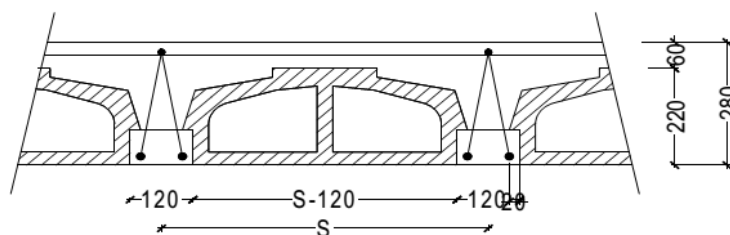


Figure 2.3: Space truss model of precast beam and slab block arrangements

The strength of the pre-cast beam-slab system depends on the strength of the individual pre-cast units and cast insitu concrete. Failure of a pre-cast beam might occur due to: (1) Yielding of the tensile (bottom) reinforcements in the pre-cast concrete block,(2) Crushing of the pre-cast concrete block under compression, (3) Failure of triangulated stirrups (buckling failure), (4) Buckling of the Compression reinforcement, (5). Shear Buckling. Depending on the grade

of concrete, grade and diameter of reinforcement, dimension of the precast beam used to produce the precast beam.

To avoid brittle, potential catastrophic failures, ductile yielding of the bottom reinforcement is the preferred failure mechanism for the final phase of the precast beam. The effect of buckling of the triangulated stirrups in the capacity of the pre-cast beam is not insignificant not to be considered. In fact, the diameter and clear height of the shear reinforcement limits the strength against buckling failure.

The experimental results have shown that near to the ultimate loading the stirrups buckle pronouncedly there by undermining the role as shear connectors. The result is the loss of (full) interaction between the pre-cast concrete block and the top reinforcement of the pre-cast beam element at loads near to its ultimate.

Pre-cast concrete structures have received considerable attention in recent years. An element isolated from such a structure is subjected to membrane stresses. Since the understanding of the behavior of a reinforced concrete element is the key to the analysis of the whole structure, a softened truss model theory has been developed for the nonlinear analysis of such membrane elements (Hsu,1993). The softened truss model incorporates the three fundamental principles of the mechanics of materials: stress equilibrium, strain compatibility and constitutive laws of materials. An accurate prediction by the softened truss model depends strongly on the constitutive laws of the concrete and steel in the elements. In this study the material models taken by softened truss model approach will be presented later. The smeared stress- strain relationship for reinforcement bars are calculated using Belarbi model closer to the actual condition.

2.3. Concrete Damage Plasticity Model

Concrete damage plasticity is continuum, plasticity based, damage model for concrete. It assumes that the main two failure mechanisms are tensile cracking and compressive crushing of the concrete materials. The evolution of the yield (failure) surface is controlled by two hardening variables, ε_t^{pl} and ε_c^{pl} , linked to failure mechanism under tension and compression loading ,respectively (Li-Jian, 2013).

2.3.1. Uniaxial tension and compression stress behavior

The model assumes that the uniaxial tensile and compressive response of concrete is characterized by damaged plasticity, as shown in Figure 2.4. Under uniaxial tension the stress- strain response follows a linear elastic relationship until the value of the failure stress, f_{tm} is reached. The failure stress corresponds to the onset of micro- cracking in the concrete material. Beyond the failure stress the formation of micro-cracks is represented macroscopically with a softening stress-strain response, which induces strain localization in the concrete structure. Under uniaxial compression the response is linear until the value of initial yield stress, $\sigma_{co} = 0.4f_{cm}$, In the plastic regime the response is typically characterized by stress hardening followed by strain softening beyond the ultimate stress, $\sigma_{co} = f_{cm}$. This representation, although somewhat simplified, captures the main features of the response of concrete.

It is assumed that the uniaxial stress-strain curves can be converted into stress versus plastic-strain curves. (This conversion is performed automatically by ABAQUS from the user-provided stress versus “inelastic” strain data, as explained below). Thus,

$$\sigma_t = \sigma_t(\varepsilon_t^{pl}, \bar{\varepsilon}_t^{pl}, f_i) \quad \text{Eq. 11}$$

$$\sigma_c = \sigma_c(\varepsilon_c^{pl}, \bar{\varepsilon}_c^{pl}, f_i) \quad \text{Eq. 12}$$

Where the subscripts t and c refer to tension and compression, respectively; ε_t^{pl} and ε_c^{pl} are the plastic strains, $\bar{\varepsilon}_t^{pl}$ and $\bar{\varepsilon}_c^{pl}$ are the equivalent plastic strain rates, and $f_i (i = 1, 2, 3, \dots)$ are other predefined field variables.

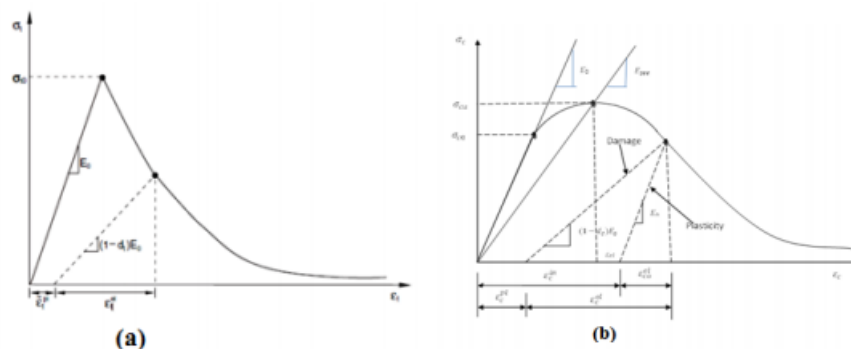


Figure 2.4: Response of concrete to uniaxial loading in (a) Tension; (b) Compression

As shown in Figure 2.4, when the concrete specimen is unloaded from any point on the strain softening branch of the stress-strain curves, the unloading response is weakened: the elastic stiffness of the material appears to be damaged (or degraded). The degradation of the elastic

stiffness is characterized by two damage variables, d_t and d_c , which are assumed to be functions of the plastic strains, temperature, and field variables:

$$d_t = d_t(\varepsilon_t^{pl}, f_i) \quad 0 \leq d_t \leq 1 \quad \text{Eq. 13}$$

$$d_c = d_c(\varepsilon_c^{pl}, f_i) \quad 0 \leq d_c \leq 1 \quad \text{Eq. 14}$$

The damage variables can take values from zero, representing the undamaged material, to one, which represents total loss of strength.

If E_o is the initial (undamaged) elastic stiffness of the material, the stress-strain relations under uniaxial tension and compression loading are, respectively (ABAQUS, 2014):

$$\sigma_t = (1 - d_t)E_o(\varepsilon_t - \varepsilon_t^{pl}) \quad \text{Eq. 15}$$

$$\sigma_c = (1 - d_c)E_o(\varepsilon_c - \varepsilon_c^{pl}) \quad \text{Eq. 16}$$

2.4. Description of Experimental Test

An experimental investigation of scaled pre-cast concrete beam was conducted. The test program was intended to study the behavior of pre-cast beam elements in order to investigate the response under load of pre-cast slab system while the cast insitu concrete is still in its plastic state by Kebede in 2009. The experimental testing program includes the construction of six simple supported precast concrete beams followed by testing them under static loading to failure.

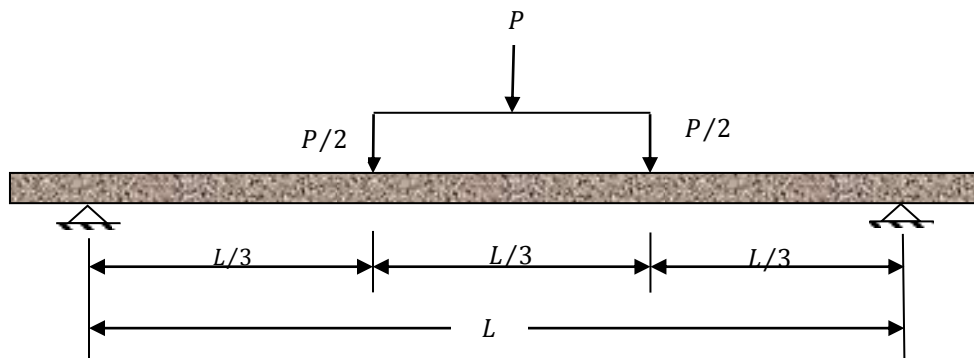


Figure 2.5: Two Point Loading

In all these beams, the width, b , the overall depth, H , and the precast block, h , was taken as 120mm, 260mm, and 80mm, respectively. These entire beams were subjected to concentrated load which was applied at $0.33L$ difference from the support to ensure that the support and the two point plates are subjected to high stresses leading to failure on parts of the precast beam. Figure 2.5 shows beam dimensions and a schematic diagram of two point

loading arrangement, while Figure 2.5 shown of the precast beam setup before testing. The following subsections summarize the description of beam groups, materials properties, and test setup and test procedure.



Figure 2.6: Photo of Test Specimens: (a) Photo of Bending Test setup and Specimens; (b). Photo of Buckled Stirrups (Kebede M, 2009)

The reinforcement detail of pre-cast concrete beams was designed in the experimental study. The pre-cast concrete beams which require the bottom reinforcement, top reinforcement and stirrups. The experimental study provided the same cross section of precast beam, different of main reinforcement bars, stirrups (shear reinforcement), and span length of the precast beam detail.

CHAPTER THREE

RESEARCH METHODOLOGY

3.1. Analysis and Modeling of Pre-cast Beam

This study considered unified theory of concrete structure subjected to various types of membrane stresses and including biaxial tension–compression. The objectives of the study to improve the mathematical expression for the constitutive laws required in the softened truss model such as smeared stress-strain relationship for concrete in tension and compression and the smeared stress–strain relationship of mild steel bars embedded in concrete.

Finite element analysis of pre-cast concrete beam subjected to static load using ABAQUS6.14. Material property, support condition and loading condition that used in the experiment used for validation were applied in the finite model of this study. Load- deflection response, buckling of stirrups and failure model were parameters used to validate. The loads were applied in the pre-cast beam according to the experimental study used for validation. After checking the finite element model reflects the real world result, the parametric study and sensitivity analysis were carried out by considering five parameters that are concrete strength, precast beam span length, sensitivity of parameter, concrete dilation angle, and viscosity parameters.

3.1.1. Description of Reference Tests specimen for validation Kebede M. (2009)

In Kebede M. six simple supported precast concrete beams followed by testing them under static loading to failure. The tested beam where divided by two groups with respect to the amount reinforcement at the top and bottom, and stirrup at the pre-cast beam, and different span length, L. In all these beams, the width ,b, the overall depth, H, and the pre-cast concrete block, h, was taken as ,120mm, 260mm, and 80mm respectively. Pre-cast beam group-I the span (L=3.5m) consisted of beams, namely: PCB-1, PCB-2 and PCB-3; Group-II the span length (L=3.0m) consisted of beams: PCB-4, PCB-5 and PCB-6. (Figure 3.1) Such group aims at assessing the major difference of ultimate load-carrying capacity and failure model.

The concrete cube compressive strength used for the casting of beams was 27.8MPa. A 12mm steel bar was used for top and bottom reinforcement, while 6mm bar was used for stirrup. Pre-cast beam group-I the bottom reinforcement, stirrups, and top reinforcement, was

taken as, $2\phi_{12mm}$, ϕ_{6mm} and ϕ_{12mm} respectively; and group-II pre-cast beams the amount of reinforcement at bottom, the amount reinforcement at top, and stirrups was taken as $2\phi_{12}$, ϕ_{12} and ϕ_{6mm} respectively.

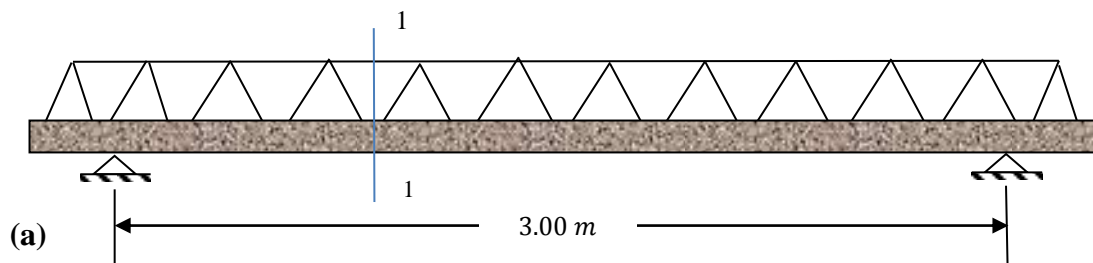
3.1.2. Descriptions of Specimen

This study used finite element analysis of pre-cast concrete beam subjected to static load using ABAQUS6.14. Material property, support condition and loading condition that used in the experiment used for validation were applied in the finite model of this study. Load-deflection response, buckling of stirrups and failure mode were parameters used to validate. The loads were applied in the pre-cast beam according to the experimental study used for validation.

In this study Pre-cast concrete beam in span length of 3m, and 3.5m with a cross-section of 120mm x 80mm were analyzed and modeled to test load deflection and bucking of stirrup using finite element analysis. The test were grouped based on span length and material properties i.e. Span length of 3.5m, depth ($h=80mm$), and width ($b=120mm$), top and bottom reinforcement of 12mm; stirrups of 6mm for PCB-2; span length of 3.5m, depth ($h=80mm$), and width ($b=120mm$), top and bottom reinforcement of 12 mm (Table 1 and Figure 3.1) C-20 , C-25 , and C-30 concrete grade is used. The yield strength and elastic modulus of reinforcement was 400 MPa and 200Gpa respectively.

Table 1: Details of specimen

Specimen Groups	Span length ,L,(mm)	Width ,b,(mm)	Depth ,d,(mm)	Top reinforcement	Bottom reinforcement	Stirrups	h_s (mm)
Group-I	3.00	120	80	ϕ_{12mm}	$2\phi_{12mm}$	ϕ_{6mm} c/c 150mm	180
Group-II	3.50	120	80	ϕ_{12mm}	$2\phi_{12mm}$	ϕ_{6mm} c/c 150mm	180



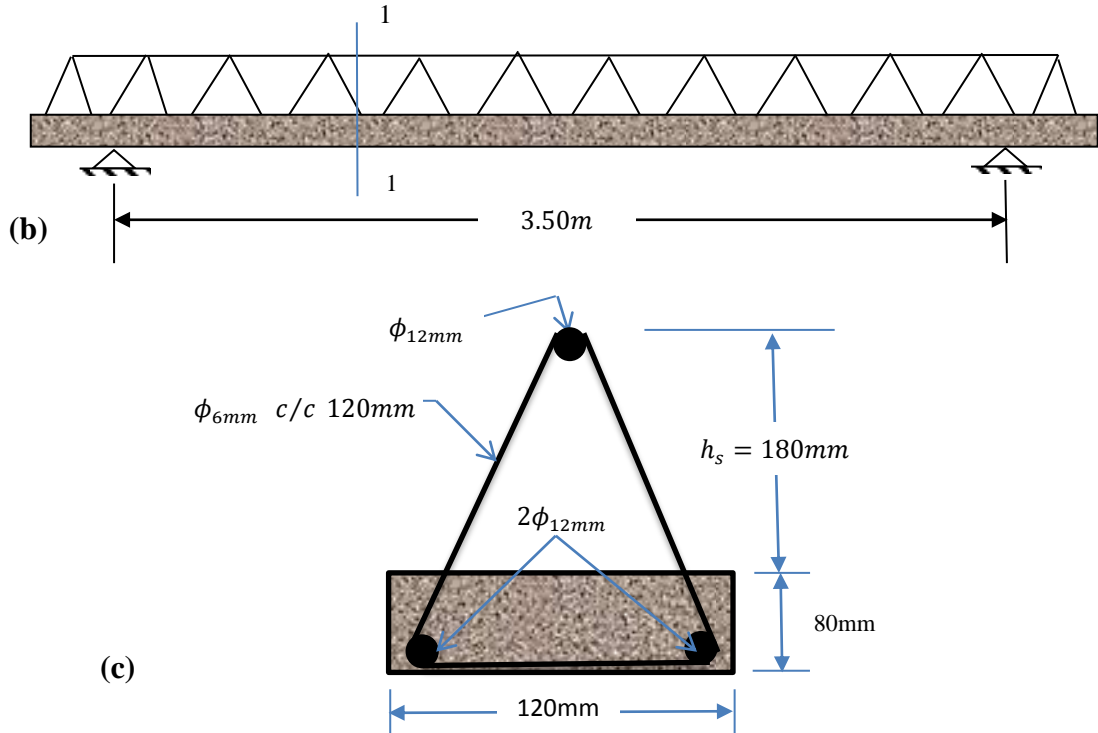


Figure 3.1: Specimen of pre-cast Concrete beams: (a) For Group-I; (b) For Group-II; and (c) precast beam cross-section 1-1.

3.1.3. Nonlinear constitutive behavior of concrete and steel bars analysis using unified theory of concrete

The unified theory of concrete structure subjected to various types of membrane stresses, including biaxial tension – compression and pure shear loadings. The objectives of the study to improve the mathematical expression for the constitutive laws required in the softened truss model. Based on this study, the following constitutive laws were derived.

3.1.3.1. Softened stress-strain relationship of concrete in compression

The primary characteristic of the constitutive law of concrete in compression is the softening of peak stress in comparison to the companion cylinder. The softening coefficient was also found to be inversely proportional to $\sqrt{f_{cm}}$. The function f_1 of equation (7) is mathematically expressed as follow (Belarbi and Hsu, 1994):

The ascending branch of the softened stress–strain curve can be expressed as:

$$\sigma_c = \zeta f_{cm} \left[2 \left(\frac{\varepsilon_c}{\zeta \varepsilon_0} \right) - \left(\frac{\varepsilon_c}{\zeta \varepsilon_0} \right)^2 \right] \quad \frac{\varepsilon_c}{\zeta \varepsilon_0} \leq 1 \quad \text{Eq. 17}$$

The descending branch of the softened stress–strain curve is calculation:

$$\sigma_c = \zeta f_{cm} \left[1 - \left(\frac{\varepsilon_c / \zeta \varepsilon_o - 1}{2/\zeta - 1} \right)^2 \right] \quad \frac{\varepsilon_c}{\zeta \varepsilon_o} \geq 1 \quad \text{Eq. 18}$$

The compressive stress σ_c calculated by Equation (17) and (18) should be limited to $0.4\zeta f_{cm}$, based on literature (Thomas T.C, 2010).

Where ε_o is the strain at the peak stress of standard concrete cylinder taken usually as 0.002 for normal strength concrete and 0.0024 for high-strength concrete, and ζ is the softened coefficient taken as follows (Zhang, 1995):

$$\zeta = \frac{5.8}{\sqrt{f_{cm}}} \frac{1}{\sqrt{1 - 400\varepsilon_r}} \quad \text{Eq. 19}$$

3.1.3.2. Smearred stress-strain relationship of concrete in tension

Smearred stress-strain relationship for concrete in tension was derived, concrete was found to develop substantial tensile stresses even after extensive cracking, and function f_2 of equation (8) is expressed mathematically as follows (Belarbi and Hsu, 1994); There are two parts of the concrete behavior:

Before crack

$$\sigma_t = E_c \varepsilon_t \quad \varepsilon_t \leq \varepsilon_{cr} \quad \text{Eq. 20}$$

After crack

$$\sigma_t = f_{cr} \left(\frac{\varepsilon_{cr}}{\varepsilon_t} \right)^{0.4} \quad \varepsilon_t > \varepsilon_{cr} \quad \text{Eq. 21}$$

Where: E_c is modulus of elasticity of concrete, f_{cr} is cracking tensile strength of the concrete, take as $f_{cr} = 0.31(f_{cm})^{2/3}$; $f_{cm} = f_{ck} + 8MPa$ (f_{ck} is the characteristic value of concrete compressive strength); and ε_{cr} stands for strain at concrete cracking (average tensile strain at which the concrete begins cracking strain of concrete, ε_{cr} taken as 0.00008 mm/mm) Equation (20) and (21) is expressed graphically in figure 4.1. Since tension

stiffening may considerably affect the results of the analysis and the relation needs calibrating for a given simulation, it is proposed to use the modified Wang & Hsu (1995) formula for the weakening function:

$$\sigma_t = f_{cr} \left(\frac{\varepsilon_{cr}}{\varepsilon_t} \right)^n \quad \text{if } \varepsilon_t > \varepsilon_{cr} \quad \text{Eq. 22}$$

Where: n represents the rate of weakening.

3.1.3.3. Reinforced bars embedded in Concrete and Smeared Stress-Strain Curves

The stress-strain relationship of mild bar tested in bare condition exhibits a long plateau after yielding. However, the smeared stress curve of steel bars embedded in concrete does not show such a yield plateau. The smeared (average) stress at first yield called “apparent yield stress(f_y^*)” and the smeared stresses in the post-yield rang were found to be lower than those of bare bar. This reduction of steel stress was found (Belarbi and Hsu, 1994) to directly related to a parameter $B = (1/\rho) (f_{cr}/f_y)^{1.5}$ expressed in terms of steel and concrete tensile strengths (f_y and f_{cr}) as well as the reinforcement ratio (ρ).

3.1.3.3.1. The Property of Steel Bars Embedded in Concrete

The real yield strength of steel bar embedded in concrete can be calculated by next formula (Belarbi and Hsu, 1995), this nearly linear relationship can be closely approximated by the following expression:

$$\frac{f_y^*}{f_y} = 1 - \frac{4}{\rho} \left(\frac{f_{cr}}{f_y} \right)^{1.5} \quad \text{Eq 23}$$

The smeared stress–strain relationship of mild steel bars embedded in concrete is more difficult to determine after yielding, because the steel strain at the cracked sections increases rapidly to reach the strain hardening region of the stress–strain curve. The averaging of the steel strains and the corresponding steel stresses along the length, L becomes mathematically more complex. The integration process involved in the averaging requires numerical integration and the use of an electronic computer.

3.1.3.3.2. Tamai et al. Model for Smeared Stress–Strain Curve

The property of steel bars embedded in concrete with these two assumptions, the smeared (averaging) process by **Tamai et al. Model** (1987).

- (a) From the first assumption we can write

$$f_{s0} = f_s + a_s \cos \frac{2\pi x}{L} \quad \text{Eq. 24}$$

Where a_s is the amplitude of the cosine curve. At the cracked sections, $f_s(x) = f_{s0}$ and $\cos 2\pi x/L = 1$ (i. e. x equal to 0 or L)

(b) Now, using the second assumption is

$$f_s(x) = f_s + \frac{1}{\rho} f_{cr} \left(\frac{\varepsilon_{cr}}{\varepsilon_s} \right)^{0.4} \cos \frac{2\pi x}{L} \quad \text{Eq. 25}$$

From equation (25) ε_s Can be determining as:-

$$\varepsilon_s = \left(\frac{1 * \cos \left(\frac{2\pi x}{L} \right)}{f_s(x) - f_s} \right)^{2.5}, \text{ for } C - 400 \quad \text{Eq. 26}$$

3.1.3.3. Belarbi's Model for Smeared Stress–Strain Curve

The prediction of this Theoretical method can be improved if the stress distribution of the steel bar is expressed by a function closer to the actual condition. Belarbi (1991) modified the cosine function in Equation (24) by adding more terms in the following form:

$$f_s(x) = f_s + a_s \cos \frac{2\pi x}{L} + b_s \left(\sin \frac{3\pi x}{L} - 0.6 \sin \frac{5\pi x}{L} - 0.1358 \right) \quad \text{Eq. 27}$$

Where a_s is given by $a_s = \frac{1}{\rho} f_{cr} \left(\frac{\varepsilon_{cr}}{\varepsilon_s} \right)^{0.4}$ in the added terms b_s , 0.6 and 0.1358 were chosen to satisfy the boundary conditions at the cracks and at the midpoint between the cracks. The additional sinusoidal and constant terms. Determine the value of b_s using the boundary condition $f_{s0} = f_s$ at $x = 0$ and $x = L$ (equation 28).

$$b_s = 7.364 \left(\frac{f_{cr}}{\rho} \right) \left(\frac{\varepsilon_{cr}}{\varepsilon_s} \right)^{0.4} \quad \text{Eq. 28}$$

From equation (27) it easy to determine the $\varepsilon_s(x)$,

$$\varepsilon_s(x) = \left(\frac{\frac{f_{cr}(\varepsilon_{cr})^{0.4}}{\rho} \left[\cos \left(\frac{2\pi x}{L} \right) + 7.364 \sin \left(\frac{3\pi x}{L} \right) - 4.4184 \sin \left(\frac{5\pi x}{L} \right) - 1 \right]}{f_s(x) - f_s} \right)^{2.5} \quad \text{Eq. 29}$$

3.1.3.3.4. Bilinear Model for Smeared Stress–Strain Curve

The smeared stress-strain relationship of reinforcing bars embedded in concrete as bilinear model. This relationship is valid for the longitudinal reinforcements indicated by the functions f_3 and f_4 in Equation (9) and (10) and is expressed mathematically as follows.

$$f_s = E_s \varepsilon_s \quad \text{When} \quad \varepsilon_s \leq \varepsilon'_y \quad \text{Eq. 30}$$

$$f_s = (0.91 - 2B)f_y + (0.02 + 0.25B)E_s \varepsilon_s \quad \text{When} \quad \varepsilon_s > \varepsilon'_y \quad \text{Eq. 31}$$

Where:-

$$\varepsilon'_y = f'_y / E_s \quad , \quad f'_y = (0.93 - 2B)f_y \quad \text{Eq. 32}$$

$$B = \frac{1}{\rho} \left(\frac{f_{cr}}{f_y} \right)^{1.5} \quad f_{cr} = 0.31 \sqrt{f_{cm}(\text{MPa})} \quad \text{and} \quad \rho \geq 0.25\% \quad \text{Eq. 33}$$

The percentage of steel ρ should not be less than 0.25%. This $\rho_{min} = 0.25\%$, should not impose any difficulty, because it is the minimum specified by the Euro code (EN 1992-1-1, 2015) for deformed bars.

Equations (31) and (33) are quite simple to use, because they are functions of only one parameter B defined in Equation (33). These two equations are applicable to both longitudinal and transverse steel.

3.1.3.3.5. Simplified and Modified versions of the constitutive Laws

The set of constitutive laws relating smeared stresses to smeared strains, equation (24) through (33), are referred to as the accurate constitutive laws. They can be used in the analysis when the deformations and the yield strength of the structure are both important.

If a structure is subjected to static loads and the deformation of the structure is not important, then the constitutive laws can be simplified by (1) neglecting the tensile stress of concrete, giving

$$\sigma_r = 0 \quad \text{Eq. 34}$$

and (2) assuming the elastic–perfectly plastic characteristic of bare mild steel bars, giving

$$f_s = \varepsilon_s E_s \quad \text{when} \quad \varepsilon_s \leq \varepsilon_y \quad \text{Eq. 35}$$

$$f_s = f_y \quad \text{when } \varepsilon_s > \varepsilon_y \quad \text{Eq. 36}$$

Where: E_s is Modulus of elasticity of mild steel bars; f_s is a stress in mild steel bars; f_y is yield stress in mild steel bars; ε_s is strain in mild steel bars; and ε_y is yield strain in mild steel bar.

Equation (17), (18), (19),(34) and (36) are referred to as ‘‘the simplified constitutive laws’’. Equation (34) is conservative in terms of the yield strength of an element and equation (35) and (36) is unconservative, the error induced by these two relationships cancel each other so that the yield strength is correctly predicted. However, the deformations will be overestimated because the *tension stiffening effect is neglected*. Physically, this simplification implies that the smeared tensile stress-strain relationships of concrete and steel are replaced by the local stress-strain relationships at the cracks. Indeed, the tensile strength of concrete is zero at the cracks, and the stress-strain relationship of mild steel bars at the cracks does exhibit the *elastic-perfectly-plastic characteristic of the bare bars* (Thomas T.C, 2010).

A *modified version of the constitutive laws* is a simultaneous employment of the smeared tensile stress-strain curve of concrete, Equation (20) and (21), and the stress-strain curve of bare steel bars, Equation (35) and (36). The *modified constitutive laws* will take into account the *tension stiffening effect* so that the deformations are correctly evaluated but it will overestimate the strength at the first yielding of steel. As a result, this combination of *two constitutive laws* will produce an unwarranted ‘‘concrete strengthening’’, in addition to a correct reduction in deformations due to *tension stiffening effect*.

3.2. Study Variables

3.2.1. Dependent variables

Modeling of smeared stress-strain behavior of pre-cast beams.

3.2.2. Independent variables

Variables which affects the precast beam.

- Sensitivity of parameters
- Grade of concrete
- Failure load, maximum deflection
- Concrete dilation angles and viscosity parameters.

3.3. Finite element modeling

The proposed strengthened model was introduced into nonlinear finite element model ABAQUS 6.14-1, which allows for nonlinear analysis of reinforced concrete beams, and both geometric and material nonlinearity.

3.3.1. Geometric modeling

Concrete model

Concrete element was modeled as 8-noded linear hexahedral brick element with reduced integration and hourglass control (C3D8R) was used. This type of element has the capability of high convergence and reduces the computation time.

Reinforcing steel model

Reinforcement bar can be defined by three dimensional truss elements with linear shape function (B31). The elements were meshed the same approximate maximum size used in the beam part.

Loading and supporting plates model

Supporting and loading plates that transfer the reaction and loads from to the concrete elements are modeled as solid element similar to the concrete. The approximate mesh size used is similar that used for concrete and reinforcing steel bar.

3.3.2. Concrete elements

Modeling nonlinear properties of concrete in computer program is challenging and requires extensive data about the material's property. The concrete damaged plasticity model is a plasticity based model that arranges for the analysis of concrete structures under monotonic, static and/or dynamic loading. Plasticity is characterized by the permanent deformation when all loads are removed, and damage is defined by the decrease in elastic constants. Plasticity should be combined with damage to properly characterize the nonlinear behavior of concrete. Concrete is brittle material under uniaxial compression (or tension) and low confining pressure. It becomes more ductile when confining pressure is large enough to prevent crack propagation and subjected to multiaxial compression.

The Concrete Damaged Plasticity model used in the ABAQUS software is a modification of the Drucker–Prager strength hypothesis. In recent years the latter has been further modified by Lubliner, Lee and Fenves. According to the modifications, the failure surface in the deviatoric cross section needs not to be a circle and it is governed by parameter K_c . K_c is interpreted as a ratio of the distances between the hydrostatic axis and respectively the compression meridian and the tension meridian in the deviatoric cross section. The CDP model recommends to assume $K_c = 2/3$.

The shape of the plane’s meridians in the stress space changes. Experimental results indicate that the meridians are curves. In the CDP model the plastic potential surface in the meridional plane assumes the form of a hyperbola. The shape is adjusted through *eccentricity* (plastic potential eccentricity). It is a small positive value which expresses the rate of approach of the plastic potential hyperbola to its asymptote. The CDP model recommends to assume $\varepsilon = 0.1$.

Another parameter describing the state of the material is the point in which the concrete undergoes failure under biaxial compression. σ_{bo}/σ_{co} (f_{bo}/f_{co}) is a ratio of the strength in the biaxial state to the strength in the uniaxial state. The ABAQUS user’s manual specifies default $\sigma_{bo}/\sigma_{co} = 1.16$.

The last parameter characterizing the performance of concrete under compound stress is *dilation angle*, i.e. the angle of inclination of the failure surface towards the hydrostatic axis, measured in the meridional plane. Physically, dilation angle ψ is interpreted as a concrete internal friction angle. In simulations usually $\psi = 15^\circ, 30^\circ, 36^\circ, 45^\circ$ and 55° is assumed. In this study the dilation used was $\psi = 36^\circ$.

The above four parameters and viscosity parameter are used to model concrete under compound stress.

Table 2: summary of the plasticity parameters used for the CDP model

Dilation Angle , ψ	Eccentricity, ε	σ_{co}/σ_{bo}	K_c	viscosity, μ
36°	0.1	1.16	0.6667	0.0005

The concrete damaged plasticity model assumes that the two main failure mechanisms in concrete are the tensile cracking and the compressive crushing. In this model, the uniaxial tensile and compressive behaviour is characterized by damaged plasticity.

3.3.3. Compressive behavior

The stress strain relation for concrete can be obtained from unified theory of concrete smeared stress-strain in compression (section 3.1.3.1). Inelastic strains ϵ_c^{in} are used in the CDP model. It is determined using the graph from smeared stress-strain by deducting elastic part (corresponding to the undamaged material) from the total strains registered in the smeared stress-strain in compression:

$$\epsilon_c^{in} = \epsilon_c - \epsilon_{oc}^{el} \quad \text{Eq. 37}$$

Where, $\epsilon_{oc}^{el} = \sigma_c / E_o$, ϵ_{oc}^{el} =Elastic strain corresponding to the undamaged material and ϵ_c =smeared tensile strain; stands for the initial modulus of elasticity for the undamaged material. Knowing the plastic strain and having determined the flow and failure surface area one can calculate stress σ_c in Equation (17) and (18). In the unloading stage, the CDP model uses the damage parameters in compression, d_c , and they would be used to calculate the stiffness of the damage material. Plastic strain in compression is then calculated by Equation (38):

$$\epsilon_c^{pl} = \epsilon_c^{in} - \frac{d_c}{(1-d_c)} \frac{\sigma_c}{E_o} \quad \text{Eq. 38}$$

The Beriberi's Model was used as the compression model to introduce the compression behavior into the CDP model. Using the unified theory of concrete for simulation of the steel Compressive behavior in ABAQUS.

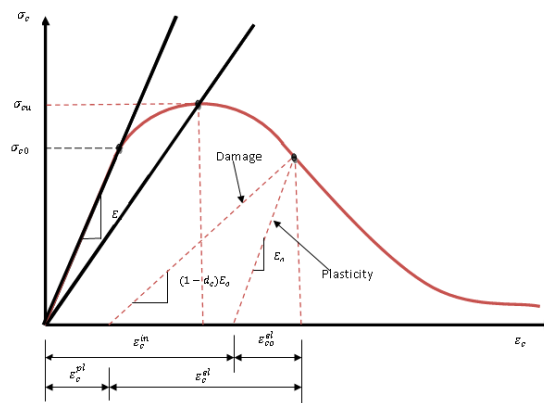


Figure 3.2: Terms for Compressive Stress-Strain Relationship /Definition of inelastic strain (Abaqus Manual, 2014)

The stress-strain relationship of the concrete in uniaxial compression can be defined in three stages. The linear elastic part of the model with initial modulus of elasticity of $E_0 = 22(0.1f_{cm})^{0.3}$ ends at the stress level of σ_{c0} ; this value was assumed to be $0.4\zeta f_{cm}$. The

stress-strain curve is then continued with a nonlinear ascending branch up to maximum compressive load ($\sigma_{cu} = \zeta f_{cm}$) which correspond to the strain of ε_o (Equation 39)

$$\varepsilon_o = 0.7(f_{cm})^{0.31} \quad \text{Eq. 39}$$

Where $f'_c = 0.9f_{cm}$, rather than the cylinder test, is used to decrease the specimen compressive strength because of compaction, shrinkage, curing, and placement. The secant modulus of elasticity can be calculated as $E_{see} = 22(0.1f_{cm})^{0.3}$. The last part of the stress strain relationship represents the softening behavior after the peak load is reached and continues up to the ultimate strain of ε_{cu} Belarbi and Hsu (1994) model.

The elastic behavior was modeled as linear and isotropic, standard values of modulus of elasticity of each concrete according to its grade and according to EBCS EN 1992-1-1: 2015. its value was calculated using the relation presented in equation (40).

$$E_{cm} = 22 \left(\frac{f_{cm}}{10} \right)^{0.3} \quad \text{Eq. 40}$$

To completely define the elastic property Poisson's ratio should have to define. From different literature position's ratio of concrete is in the ranges of 0.15 to 0.2. In this study a value of 0.18 for position's ratio was chosen.

3.3.4. Tension Stiffening Relationship

In order to simulate the complete tensile behaviour of reinforced concrete in ABAQUS, a post failure stress-strain relationship for concrete subjected to tension (similar to Figure 3.3) is used which accounts for tension stiffening, strain-softening, and reinforcement interaction with concrete. To develop this model, user should input young's modulus (E_o), smeared stress (σ_t), cracking strain (ε_t^{ck}) values and the damage parameter values (d_t) for the relevant grade of concrete.

The term cracking strain ε_t^{ck} is used in CDP model numerical analyses. The aim is to take into account the phenomenon called tension stiffening. The strain after cracking is defined as the difference between the smeared strain and the elastic strain for the undamaged material:

$$\varepsilon_t^{ck} = \varepsilon_t - \varepsilon_{to}^{el} \quad \text{Eq. 41}$$

Where, $\varepsilon_{to}^{el} = \sigma_t / E_{cm}$, ε_{to}^{el} = the elastic strain of undamaged material, σ_t smeared strain (equation 20 and 21).

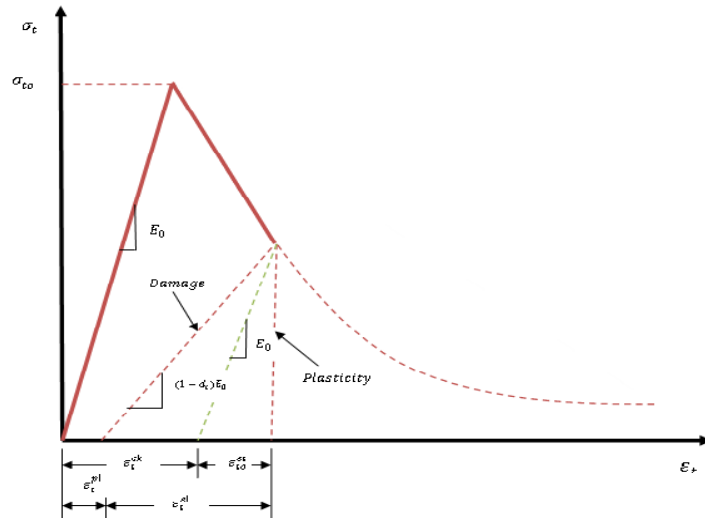


Figure 3.3: Terms for Tension Stiffening Model (Abaqus Manual, 2014)

ABAQUS (SIMULIA, 2014) checks the accuracy of damage curve using the plastic strain values (ε_t^{pl}) calculated as in Equation (42) below. Negative and/or decreasing tensile plastic strain values are indicative of incorrect damage curves which may lead to generate error message before the analysis is performed (Abaqus Manual, 2014).

$$\varepsilon_t^{pl} = \varepsilon_t^{ck} - \frac{d_t}{(1 - d_t)} \frac{\sigma_t}{E_0} \quad \text{Eq. 42}$$

3.3.5. Reinforcement bar

Under elastic analysis, plain concrete is considered in the finite element modeling since the stiffness contribution of concrete is much greater than the reinforcement but in the non-linear analysis reinforced concrete model should be considered basically in determining the ultimate capacity of a structure. In this study the reinforcing bars are modeled as beam elements that are one dimensional line elements in three dimensional space that have stiffness associated with deformation in the line. Both elastic and plastic properties were included. The elastic option used to assign the modulus of elasticity and Poisson's ratio. As well as the plastic option used to assign the smeared stress and smeared strain values that were used to model the reinforcement plastic property. Mechanical properties of reinforcing bars that are used in the validation and parametric study were directly taken from the unified theory of concrete are given the section 3.1.3.3. Therefore, the effect of shear is not neglected. To resist this shear effect we should provide diagonal reinforcement additional to longitudinal bar and stirrups. The angle of inclination is considered according to the validation experiment.

3.3.6. Loading and Boundary Condition

After modeling and assembling the section appropriate boundary condition were created using the boundary condition option using the initial step. The simple support both end of the pre-cast concrete beams using Encastre option. The loading condition used in this research was expressed in form of displacement and created using boundary condition option in the second step which was created as nonlinear dynamic explicit. The Static slandered load was applied with gradually increasing displacement amplitude using the loading spectrum shown in figure 3.4 that provides more effective data regarding the hysteretic behavior of members or structures.

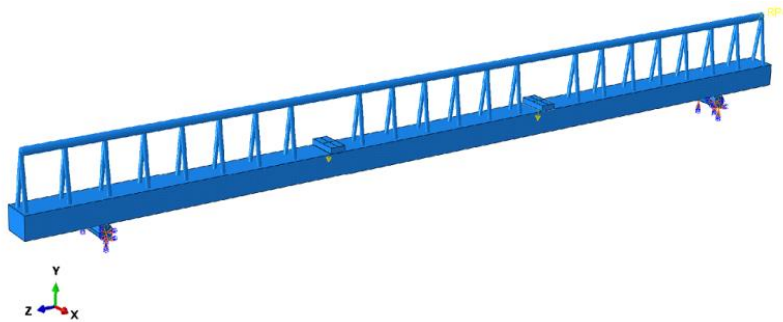


Figure 3.4: Loading and Boundary condition of Model

3.3.7. Finite Element Mesh

Material property is programmed within the mesh element, and the interaction of all elements defines the structural response as a whole system. Mesh dependency is one of the main problems when using the smeared stress -strain law to define the softening behavior of the material in compression and tensile stiffening. Application to use the mesh sensitivity problem. The type of the element, size, and arrangement has a significant effect on the numerical simulation.

Loading response of a finite element analysis depends significantly on the cracking displacement and propagation. Utilizing mesh that is too coarse in the cracking zone may result in a stiffer response than reality. On the other hand, the use of extra fine mesh may result in a softer response.

In finite element analysis, we can divide the member into many elements according to the size and shape of mesh. The size of the finite element mesh has a significant effect on the accuracy of the finite element analysis output. There are no definite rules for selecting the proper mesh size for the analysis of reinforced concrete members, testing the finite element

models with different mesh sizes are usually a good way to gain an initial understanding about the proper mesh size and the sensitivity of the results to different mesh sizes. Finer mesh may consume time for analysis and coarser mesh may yield less accurate result that does not match with actual behavior. In this study, the optimal mesh size has been found 20mm for concrete and for the reinforcement bars.

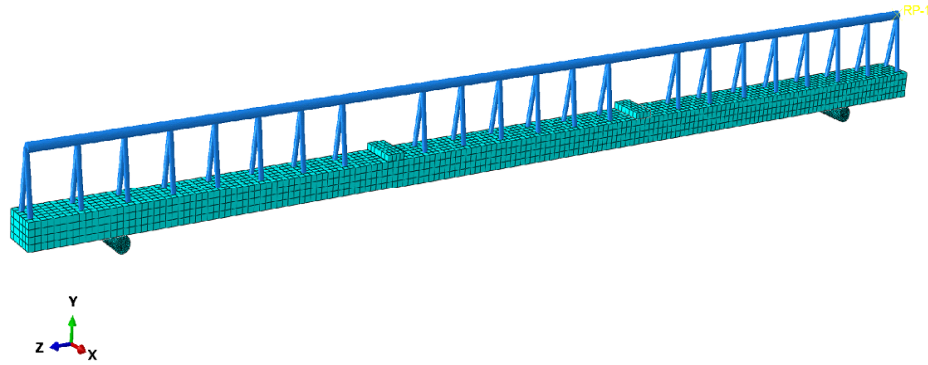


Figure 3.5: Finite Element Mesh

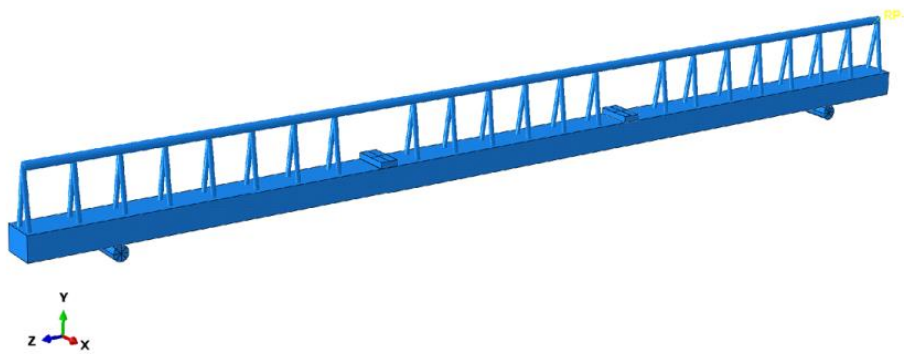


Figure 3.6: Geometric assembly of Pre-cast concrete Beam

Before defining and boundary condition interaction between two parts should be created using interaction module. Reinforcement have been modeled as embedded elements in concrete region so that the interaction between reinforcement and concrete elements assumed to be fully bonded which can be done using embedded region option under interaction module. Pre-cast concrete block and reinforcement are bonded using tie option under interaction module.

CHAPTER FOUR

RESULT AND DISCUSSION

4.1. Numerical Analysis of pre-cast beam based on unified theory

In this study the pre-cast concrete beam element section commonly used for the construction of “low cost housing” is used. To check the serviceability and ultimate limit of the pre-cast element at the initial stage (when the poured concrete is wet) and final load stage, By considering the role of the concrete using space truss model, it is better to determine the smeared tensile stress of the concrete as well as the steel using different methods such as Tamai.et al (1991), Belarbi (1994) and Bilinear. Draw the smeared (average) tensile stress – strain relation of the pre-cast beam using these methods and select the best one to use the smeared stress and strain as material property of the pre-cast beam in the ABAQUS analysis. Since Belarbi use additional constant terms and sinusoidal function which makes the result approaches to the exact over the others.

Then determine the maximum deflection of the precast beam from the ABAQUS result and compare with the test result data and allowable deflection.

4.1.1. Smeared tensile stress-strain Curve of concrete in tension

An analytical study was done Smeared tensile stress-strain relations of concrete using equation (20) to (22). The pre-caste beams section were concrete block (120mm x 80mm), concrete cover (20mm), concrete material property (C-20 , C-25 and C-30), and steel bar are deformed bar (bottom reinforcement, top reinforcement, and Stirrups).

Stress-strain curve using the weakening function (n) were plotted at different n value. Based on the analysis when value of n increased tensile stress-stain value of the concrete decreased (Figure 4.1)

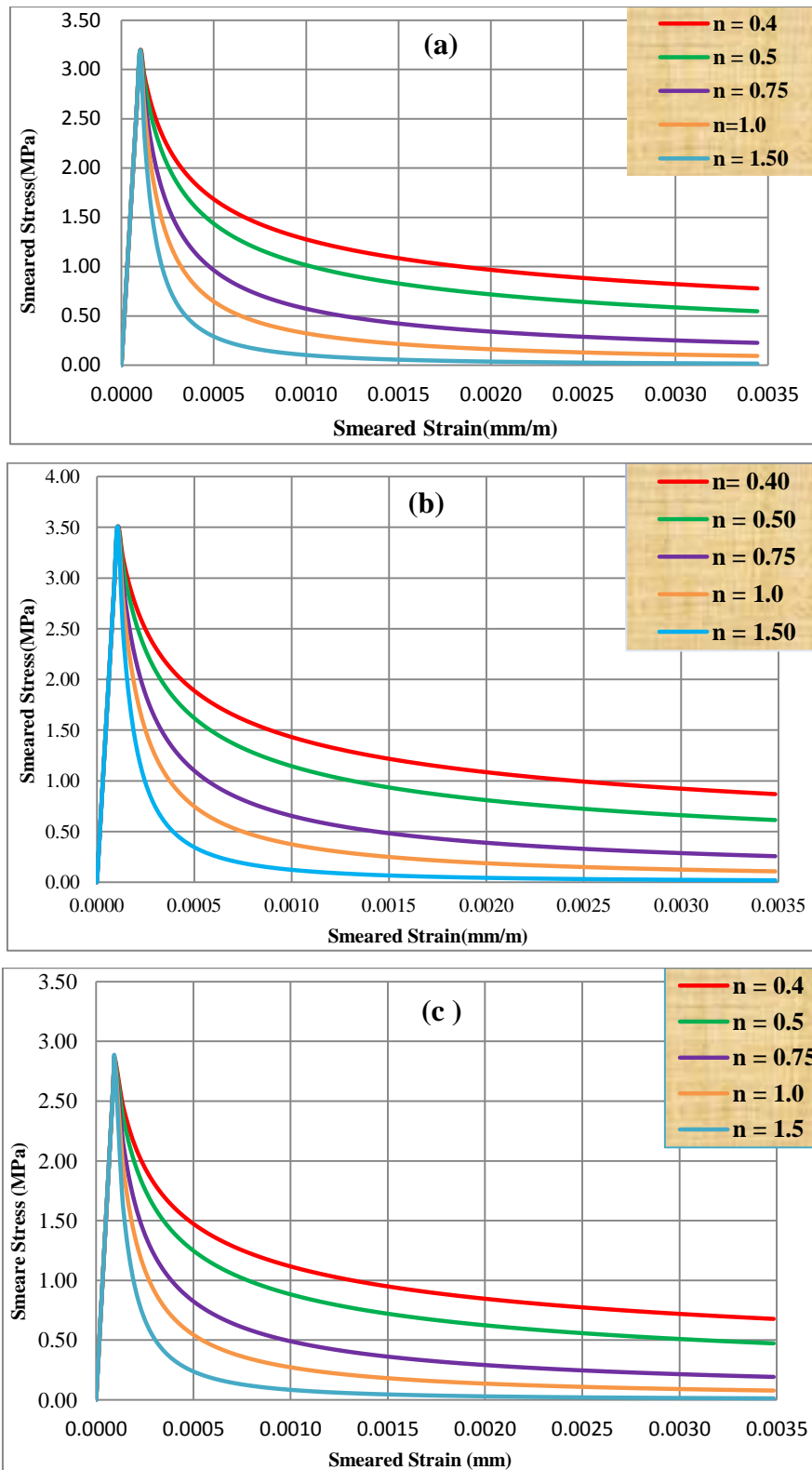


Figure 4.1: Smeared tensile stress-strain relation of concrete: (a) for grade C-25 concrete, (b) for grade C-30 concrete, (c) for grade C-20 concrete

The tensile stress of concrete σ_t is small compared with the compressive stress, but not zero. This stress σ_c is an uniform tensile stress of concrete, representing the stiffening of the steel

bars by concrete in tension. Figure 4.1 shows a typical tensile stress–strain curve of concrete. The curve consists of two distinct branches. Before cracking the stress–strain relationship is *essentially linear*. After cracking, however, a drastic *drop of strength* occurs and the descending branch of the curve becomes concave. In the descending branch, the concrete is cracked and the concept of concrete tensile stress σ_t and concrete tensile strain ε_t are quite different from those before cracking. σ_t is defined as the smeared (or average) concrete tensile stress and ε_t is the smeared (or average) concrete tensile strain. Unlike plain concrete, where the tensile stress drops directly to zero after cracking, the tensile forces in precast concrete beam continue to be resisted partially by steel, and partially by concrete between the cracks. Thus, the concrete between the cracks is still able to resist a smeared tensile stress. As the tensile load increases, more cracks form, and the cracks becomes wider, resulting in a drop in the smeared tensile stress in concrete as the smeared tensile strain increases beyond the cracking strain, as shown in figure 4.1. This concrete contribution between cracks is known as *tension stiffening*, and plays a significant role in the deformation of reinforced concrete structures.

4.1.2. Softened stress-strain curves of concrete in compression

Softened stress-strain relationship of concrete in compression as using equation (17) and (18), and Microsoft office Excel the material such as C-25, C-20 and C30 shown in Figure 4.2. There are two functions describing the curve’s ascending and descending part. They also include coefficient ζ representing the reduction in compressive stress of concrete resulting from locating reinforcing $\zeta = 1$ indicates no reinforcement taken into account. It is worth noticing that Hsu (1994) mentioned, the EN19921-1 relations almost coincide.

The consequence of this property of the parabola was either the exceedence of the concrete’s strength for a correct initial modulus value or the necessity to lower the value in order to reach a specific stress value in extreme. Figure 4.2 shows relation for Wang and Hus for grade C-20, C-25 and C-30 concrete. The following batch denotations were assumed:

- $E_{cm} - E_c = E_{cm} = 28608 \text{ MPa}$ was assumed as the initial modulus, calculated extremum $f_{cm} = 27.81 \text{ MPa}$;
- $0.4\xi f_{cm}$ –the value of initial modulus $E_c = 314876 \text{ MPa}$ matched so that the curve intersects point $(\varepsilon_c, 0.4\xi f_{cm})$, calculated extremum $f_{cm} = 33 \text{ MPa}$;

- $E_c = E_{cm}$ – a straight line describing the elastic behaviour of the concrete up to $(\epsilon_c, 0.4\xi f_{cm})$.

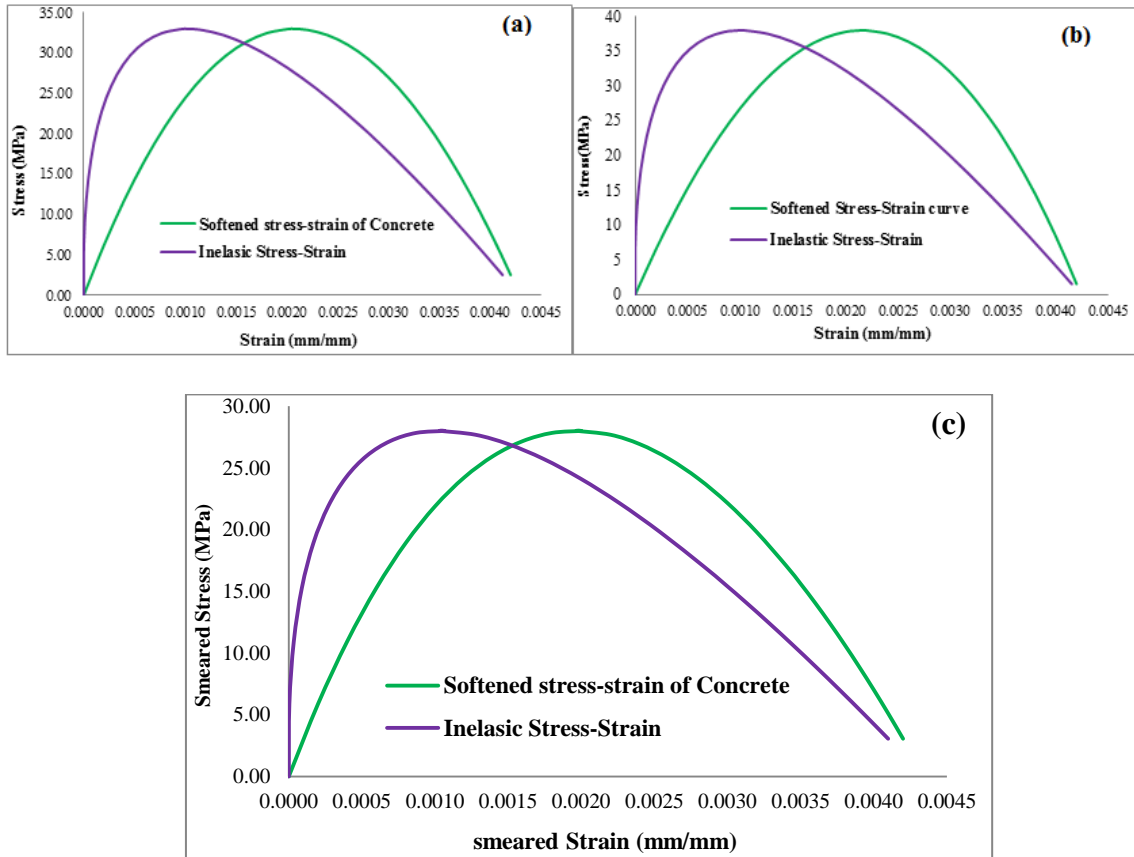


Figure 4.2: Compressive Stress-Strain curve of concrete: (a) for grade C-25 concrete,(b) for grade C-30 concrete, (c) for grade C-20 concrete

As one can see, when initial modulus E_c is assumed to amount to E_{cm} , the strength of the concrete is much overrated despite the fact that the initial modulus is still underrated (numerically E_{cm} is not the highest value). In the case parabolic relation one should artificially lower modulus E_c in order for the graph to intersect the correct value f_{cm} .

A precast beam are modeled and analyzed as a Space truss for the first three stages of construction. The modeling and analysis is done using an application of ABAQUS 6.14, software.

4.1.3. Steel bars embedded in Concrete and Smearred Stress-Strain Curves

Based on statistical analysis of analytical results with parameters of reinforcement ratio, concrete strength and steel yield strength, the look yield strength f_y^* using Equation (23) determined the stress–strain curve of bare mild steel bars and smearred yield stress of mild steel can be solved. The all of Sample of the Pre-cast concrete Beam cross-section; the

deformed bar such as bottom reinforcement, top reinforcement, and stirrups reinforcement showing in Table 3 and Figure 4.3.

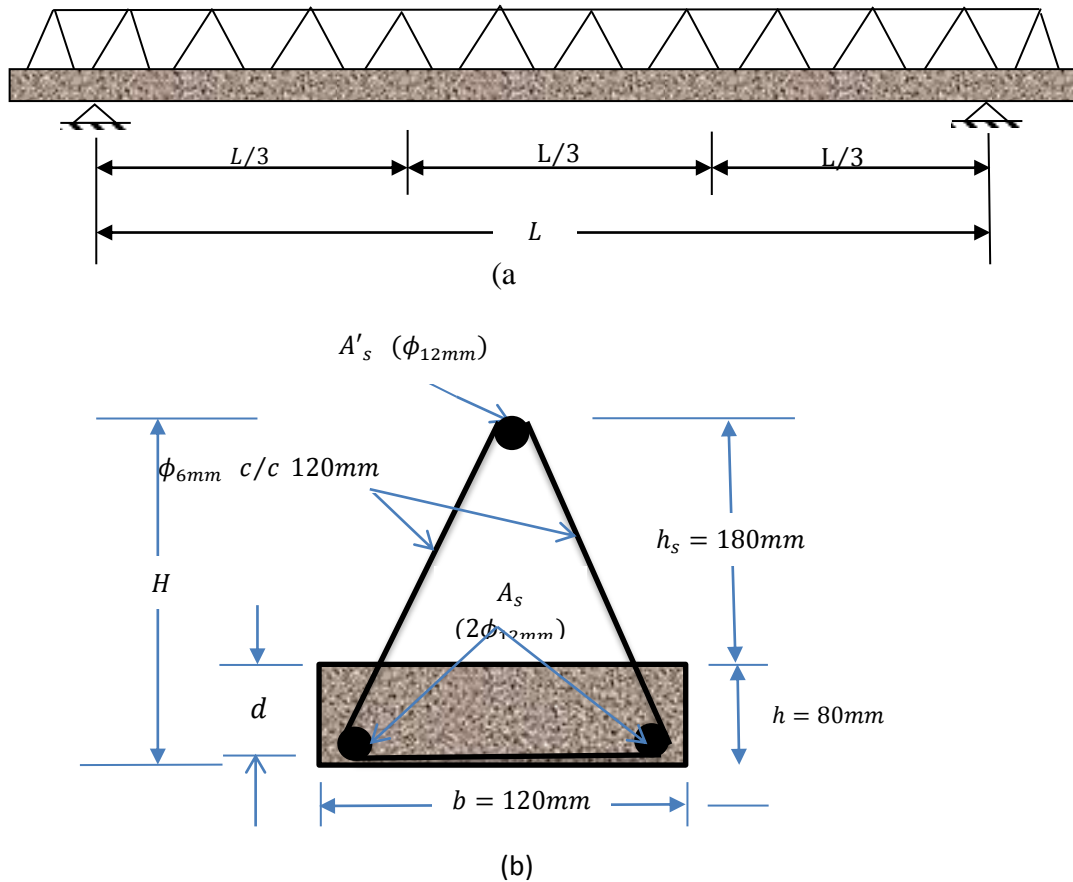


Figure 4.3: Pre-cast concrete beams: (a) longitudinal Pre-cast Beam section; (b) Beam section

Table 3: Pre-cast beam dimensions and materials of steel

Pre-cast beam	Span length ,L,(m)	Top reinforcement	Bottom reinforcement	Stirrups	b (mm)	d (mm)	h (mm)	H (mm)	h_s (mm)
Group-I	3.00	ϕ_{12mm}	$2\phi_{12mm}$	ϕ_{6mm} c/c 150mm	120	60	80	260	180
Group-II	3.50	ϕ_{12mm}	$2\phi_{12mm}$	ϕ_{6mm} c/c 150mm	120	60	80	260	180

The Pre-cast concrete Beam, PCB-2: for C-25 and S-400: Material properties:for concrete, such as $f_{cm} = 25 + 8 = 33 \text{ Mpa}$; Modulus of elasticity of steel, $E_s = 200 \text{ GPa}$; Modulus of elasticity of concrete $E_{cm} = 31475.81 \text{ MPa}$; Cracking strain of concrete $\epsilon_{cr} = 0.00008$; the bottom reinforcement $2\phi_{12}$ and the top reinforcement ϕ_{12} ; The effective depth, $d = 80 \text{ mm} - 20 \text{ mm} - 12/2 = 54 \text{ mm}$; area of concrete area of the bottom reinforcement bar, $A_s = 226.20 \text{ mm}^2$; area of the top reinforcement bar, $A'_s = 13.097 \text{ mm}^2$; and The cracking stress of concrete, take as $f_{cr} = 3.189 \text{ MPa}$; and yield strength, $f_y = 400 \text{ MPa}$; percentage ratio, $\rho = A_s/bd = 3.491\%$.

Table 4: Pre-cast beams and reinforcement quantities

Pre-cast beam	Span length (m)	d' (mm)	bd (mm ²)	A'_s (mm ²)	A_s (mm ²)	Area of stirrup(mm ²)	ρ (in %)
Group-I	3.00	54	6480	113.10	226.20	28.27	3.491
Group-II	3.50	54	6480	113.10	226.20	28.27	3.491

Table 5: Martial Property for Concrete

Concrete grade	f_{cm} (MPa)	E_{cm} (MPa)	f_{cr} (MPa)
C-28	36	32,308.250	3.367
C-30	38	32,836.568	3.504
C-25	33	31,475.806	3.189
C-20	28	29,961.951	2.766

Exact solution: $f_{cr}/f_y = 3.189/400 = 0.0079725$. The smeared yield stress of steel, f_y^* are calculated used the equation (23).

Approximate solution according to Belarbi and Hsu's Equation (23):

$$\frac{f_y^*}{f_y} = 1 - \frac{4}{\rho} \left(\frac{f_{cr}}{f_y} \right)^{1.5} = 0.918$$

$$f_y^* = 0.918 * 400 = 367.374 \text{ MPa}$$

The following Table 6 depicts the summary Material property

Table 6: Summarized Material Property for the pre-cast beams

Pre-cast beam	E_s (GPa)	ρ (in %)	$f_{cr} = 3.367 \text{ MPa}$	
			f_y^*/f_y	f_y^* (MPa)
Group-I	200	3.491	0.921	397.312
Group-II	200	3.491	0.921	397.312

Table 7: Summarized Material Property for the pre-cast beams

Pre-cast beam	A'_s (mm ²)	A_s (mm ²)	ρ (in %)	$f_y = 400 \text{ MPa}$					
				$f_{cr} = 3.189 \text{ MPa}$		$f_{cr} = 3.504 \text{ MPa}$		$f_{cr} = 2.766 \text{ MPa}$	
				f_y^*/f_y	f_y^* (MPa)	f_y^*/f_y	f_y^* (MPa)	f_y^*/f_y	f_y^* (MPa)
Group-I	113.10	226.20	3.491	0.918	367.374	0.906	362.423	0.934	373.645
Group-II	113.10	226.20	3.491	0.918	367.374	0.906	362.423	0.934	373.645

In this study using equation (24) through (26), (35) & (36) and numerical method, smeared (average) stress-strain relation of precast concrete beam bar can be solved. Figure 4.5 is a

sample, PCB-2, the section is the pre-cast concrete beams section shown in and Table 3 is Concrete block is 120 mm x 80 mm and concrete cover 20mm shown in Figure 4.3 (b), the steel bars material property are S-400, and steel bar is deformed bar such as bottom Reinforcement and top reinforcement are shown in Table 3. Using the above algorism in micro soft excel determine a series of smeared tensile stresses and strains of the mild steel using the Pre-cast concrete beam by Tamai model.

4.1.4. Belarbi’s Model for Smeared Stress–Strain Curve of Mild steel

In this study the pre-cast concrete beams PB-2 using equation (27) and (29). For materials property. $f_{cr} = 3.189MPa$, $\rho = 3.491\%$., and in equation (28) the value and equation (29) to determine the. Using Micro excel determined the smeared (average) stress-strain relation of mild steel shows in Figure.4.4 shows the variation by parameter of reinforcement ratio, ρ , and the shows the variation by parameter of concrete strength.

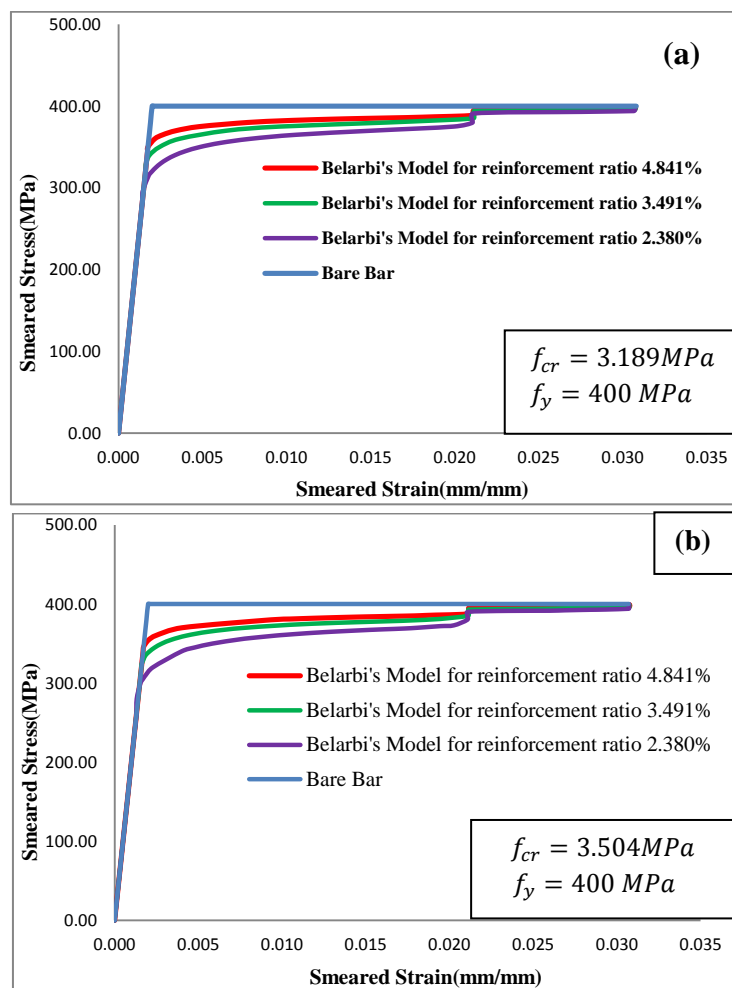


Figure 4.4: Smeared stress-strain curves of mild steel

In Figure 4.4 is plotted as a function of ρ and f_{cr} . Figure 4.4 reveals two trends: First, the lower the percentage of steel ρ , the lower the yield stress ratio. This ratio f_y^*/f_y is particularly sensitive to ρ at low percentages of steel. Second, the higher the value of, the lower the smeared yield stress ratio. Physically, both trends express the fact that the steel bar in Figure 2.2 is receiving more help from the concrete to resist the tensile force P .

The peak-softening coefficient is primarily a function of the principal tensile strain, and the concrete strength. For reinforced steel, the first stress of the smeared stress-strain curve is lower than that of a bare bar. The smeared (or average) stress-strain relationship of steel bars embedded in concrete is given by a Belarbi model expressed by Equation (27) through (29). Incorporating this set of accurate constitutive laws into the softened truss model will produce an accurate prediction of load-deformation response throughout the loading.

4.1.5. Bilinear Model for Smeared Stress–Strain Curve

In calculating the parameter B in Equation (33), the percentage of steel ρ should not be less than 0.25%. This $\rho_{min} = 0.25\%$ should not impose any difficulty, because it is the minimum specified by the Euro code (EN 1992-1-1) for deformed bars.

In this study these two equations were used in pre-cast beam (Table 3) Concrete block and for the material steels S-400, concrete C-25, the steel ratio, $\rho = 3.491\% > 0.25\%$, this is ok for analysis and yield strength; ; $f_y = 400\text{MPa}$; $f_{cr} = 3.189\text{MPa}$; , and $E_s = 200\text{GPa}$. .
Find: smeared steel stress f_s at a smeared tensile strain

$$B = \frac{1}{\rho} \left(\frac{f_{cr}}{f_y} \right)^{1.5} = 0.0203912$$

$$f_y' = (0.93 - 2B)f_y = [0.93 - (2 * 0.0203912)]f_y = 355.68\text{MPa}$$

$$\varepsilon_y' = \frac{f_y'}{E_s} = 0.0017784$$

Since $\varepsilon_s = 0.01 > 0.0017784 = \varepsilon_y'$, use equation (44)

$$f_s = (0.91 - 2B)f_y + (0.02 + 0.25B)E_s\varepsilon_s = 356.614\text{MPa}$$

For calculated value,

$$\frac{f_y'}{f_y} = 0.43 + 0.5 \frac{f_y^*}{f_y}$$

$$\Rightarrow \frac{356.614}{400} = 0.43 + 0.5 \frac{f_y^*}{400}$$

$$\Rightarrow 0.8915 - 0.43 = 0.5 \frac{f_y^*}{400}$$

$$\Rightarrow f_y^* = \left(\frac{(0.8915 - 0.43)}{0.5} \right) 400 = 0.9231 * 400 = 369.228 \text{ Mpa}$$

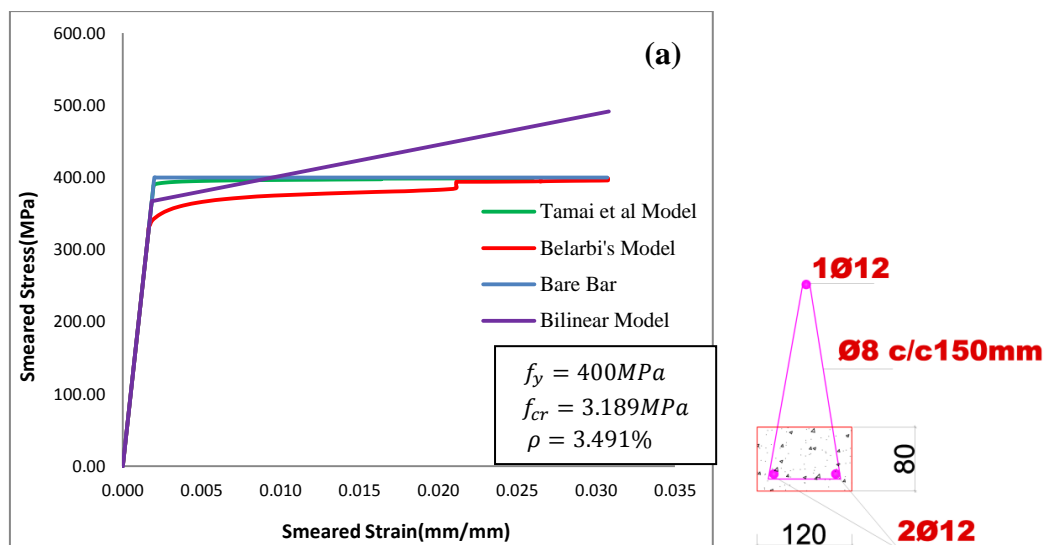
Table 8: Summarized Materials Property by Bilinear Model

Pre-cast Beam	E_s (GPa)	ρ (in %)	$f_y = 400 \text{MPa}$		
			B	f_y^* (MPa)	ϵ_s (mm/mm)
Group-I	200	3.491	0.01975	384.158	0.0019208
Group-II	200	3.491	0.01975	384.154	0.0019208

Table 9: Summarized Materials Property by Bilinear Model for different crack strength

Precast beam	E_s (GPa)	ρ (in %)	$f_{cr} = 3.189 \text{MPa}$			$f_{cr} = 3.504 \text{MPa}$			$f_{cr} = 2.766 \text{MPa}$		
			B	f_y' (MPa)	ϵ_s (mm/mm)	B	f_y' (MPa)	ϵ_s (mm/mm)	B	f_y' (MPa)	ϵ_s (mm/mm)
Group-I	200	3.491	0.02039	355.69	0.001778	0.02349	353.21	0.001766	0.016472	358.82	0.001794
Group-II	200	3.491	0.02039	355.69	0.001778	0.02349	353.21	0.001766	0.016472	358.82	0.001794

From equation (24) through (36) was used algorithm in Microsoft Excel to determine a series of smeared stresses.



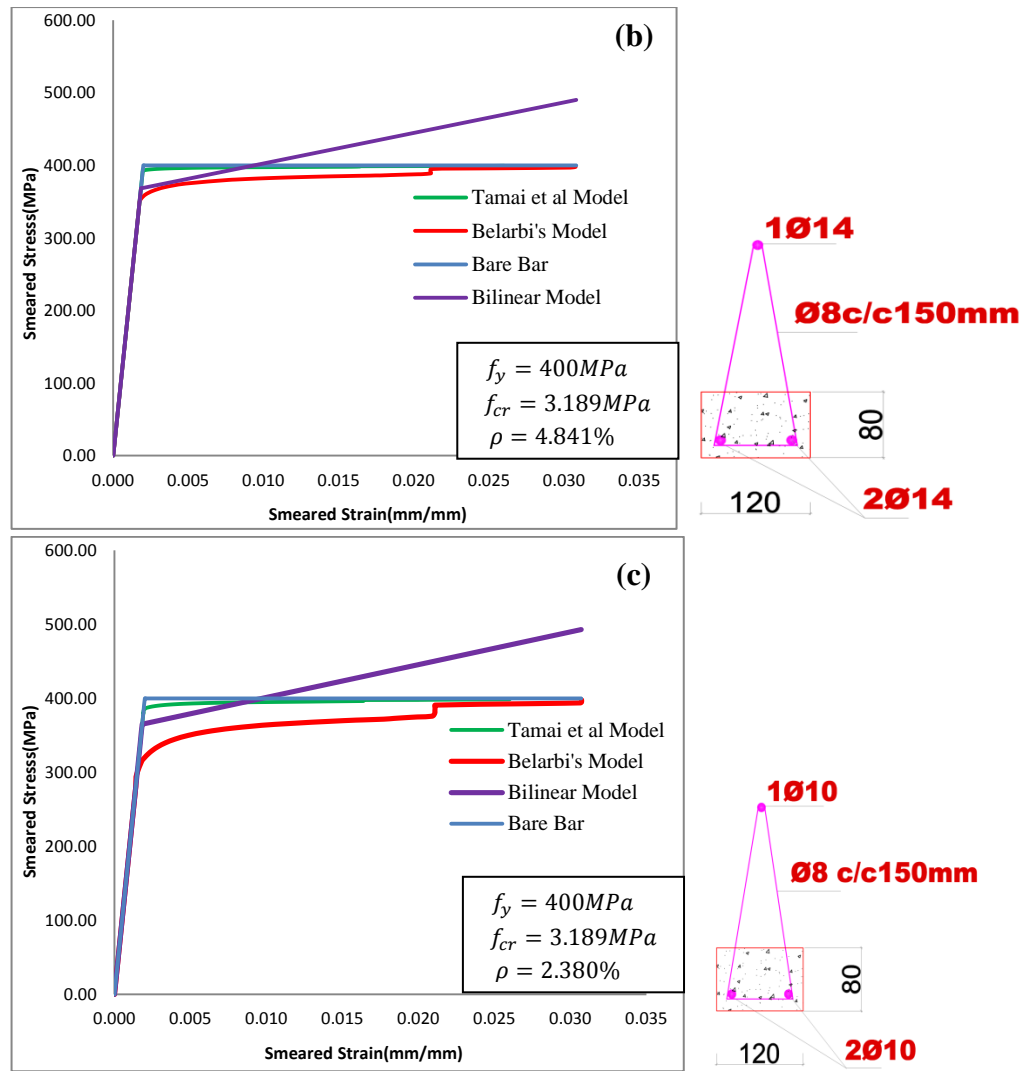


Figure 4.5: Smeared Stress-Strain Curve of mild steel for percentage of steel (ρ) and cracking strength of concrete (f_{cr}) as parameter.

A parametric study using Belarbi's method was carried out to examine the effect of the percentage of steel ρ and the cracking strength of concrete f_{cr} on the post-yielding stress-strain curves of steel. Figure 4.5 (a) and (b) gives a family of stress-strain relation using the percentage of steel ρ as parameter and the cracking strength of concrete f_{cr} as parameter. It can be seen that the smeared stress-strain curves move downward when ρ is decreased and when f_{cr} is increased.

Then to check the serviceability and ultimate limit of the pre-cast element at the initial stage and final load stage, we considered the role of the concrete using different methods such as Tamai et al (1991), Belarbi (1994) and Bilinear. The smeared tensile stress-strain relation of the pre-cast beam using those methods and selecting the best one to use the smeared stress and strain as material property of the pre-cast beam in the ABAQUS analysis. Since Belarbi

use additional constant terms and sinusoidal function which makes the result approaches to the exact over the others. Then, to determine the maximum deflection of the precast beam from the ABAQUS result and compare with the test result data and allowable deflection.

Table 10: Selected of Smeared Stress and Smeared Strain of Mild steel from three model for grade C-25 concrete

Steel ratio,(in %)		Tamai et al Model	Belarbi's Model	Bilinear Model
3.491	From graph	388.000	320.000	370.220
	Calculated Value	367.374	386.382	355.687
		397.312*	397.312*	384.158*
4.841	From graph	391.000	345.00	367.000
	Calculated Value	390.651	390.651	360.236
2.380	From graph	380.000	320.000	362.020
	Calculated value	352.144	352.144	348.072

* Experimental value

Table 11: Selected of Smeared Stress and Smeared Strain of Mild steel from three model for grade C-30 concrete

Steel ratio,		Tamai et al Model	Belarbi's Model	Bilinear Model
3.491	From graph	393.524	315.000	366.640
	Calculated Value	362.423	362.423	353.210
4.841	From graph	391.000	355.000	368.140
	Calculated Value	372.902	372.902	358.450
2.380	From graph	385.000	260.000	364.140
	Calculated value	344.881	344.881	344.440

Table 12: Selected of Smeared Stress and Smeared Strain of Mild steel from three model for grade C-20 concrete

Steel ratio,		Tamai et al Model	Belarbi's Model	Bilinear Model
3.491	From graph	398.000	340.000	380.220
	Calculated Value	373.645	373.645	358.823
4.841	From graph	391.000	320.000	367.000
	Calculated Value	380.995	380.995	362.497
2.380	From graph	380.000	345.000	360.000
	Calculated value	361.343	361.343	352.671

From the Table 10 , 11 and 12 it is better to take the values of Smeared Stresses and Smeared Strains of Belarbi Model so as insert in nonlinear material in the ABAQUS 6.14 analysis, because its smeared stress is the smallest of all.

In this study the reinforcing bars are modeled as beam elements that are one dimensional line elements in three dimensional space that have stiffness associated with deformation in the line. Both elastic and plastic properties were included. The elastic option used to assign the modulus of elasticity and Poisson's ratio. As well as the plastic option used to assign the smeared stress and strain values that were used to model the reinforcement plastic property. Mechanical properties of reinforcing bars that are used in the validation and parametric study were directly taken from the experimental program and are given the table 3. The mechanical properties of reinforcement used in the systematic study were from the combination obtained from unified theory of concrete the smeared stress–strain relationship of mild steel bars embedded in concrete. Pre-cast concrete beams and considered the effect of shear is used in dilation angle of materials. To resist this shear effect we should provide diagonal reinforcement additional to longitudinal bar and stirrups. The angle of inclination is considered according to the validation experiment. The selected of smeared stress and smeared strain of mild steel.

The precast beam is modeled and analyzed as space truss like a roof truss with reinforcement as its member. This Space truss investigated in three different stages of construction: Placement of precast beam, block laying stage, concrete pouring stage and final or working stage. In the final stage since the concrete gets hardened, the structure can be treated as a usual Pre-cast concrete beam.

4.2. Modeling and Analysis of Precast Beam

A precast beam is modeled and analyzed as a space truss for the first three stages of construction. In fact it is difficult to determine analytically the load at which buckling failure of the stirrups occur, structural software like ABAQUS 6.14 can be used to analyze the truss Model loading successively with higher loads until bucking failure of the legs of the stirrups occur. The moment capacity of pre-cast beam consists of two parts,

- Moment from couple, which consists of compression from the upper fibers of precast concrete block stressed under compression together with tension from the tensile reinforcement at the bottom.
- Moment from the couple, which consists of compression from the top reinforcement and tension from the longitudinal shear that arises in the legs of shear reinforcements just above the pre-cast concrete block as shown figure 4.6.

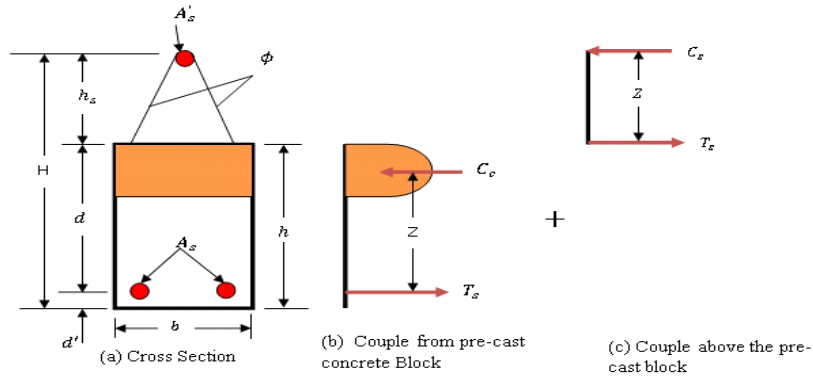


Figure 4.6: Model for Analysis and Design.

4.2.1. Analysis of Pre-cast Concrete Block

From experimental observation, failure of the pre-cast block occurs (after pronounced buckling of stirrups) by crushing of the top fibers of concrete. For compression failure, the criterion is that the compression strain in the concrete becomes. The steel stress, not having reached the yield point, is proportional to the steel strain,.

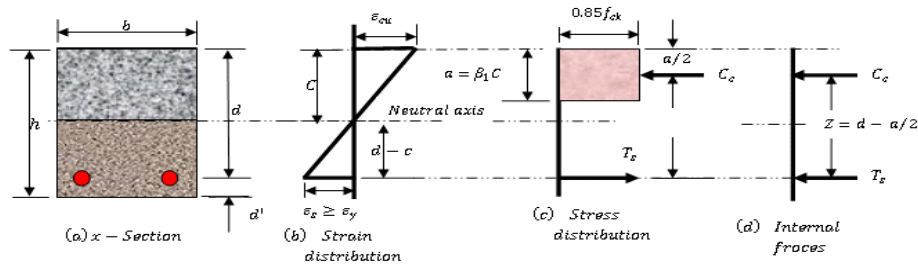


Figure 4.7: Stress and strain Profile for pre-cast concrete block

In this study used tension-controlled section, we can compare the depth to the neutral axis, C in figure 4.7, which is the limit on the neutral axis depth for tension-controlled sections. Equation (45) will be used to determine the depth of the compression stress block for the selected tension steel area. The values of the tension and compression forces are shown in Figure 4.7(d). The concrete compression force is equal to the volume under the stress block. For the rectangular section used here,,

$$C_c = 0.85 a b f_{ck} \quad \text{Eq. 43}$$

Equilibrium required that

$$C_c = T_s \quad \text{Eq. 44}$$

$$0.85 a b f_{ck} = A_s f_y$$

The depth of the stress block .So, solving for the unknown value of “a”

$$a = \frac{A_s f_y}{0.85 b f_{ck}} \quad \text{Eq. 45}$$

and then, using $\beta_1 = 0.8$ the depth to the neutral axis is

$$c = \frac{a}{\beta_1} \quad \text{Eq. 46}$$

From similar triangles in the linear strain distribution in Fig. 4.7b, the following expression can be derived

$$\epsilon_s = \left(\frac{(d - c)}{c} \right) \epsilon_{cu} \quad \text{Eq. 47}$$

The ultimate moment of the precast concrete block that failure occurs by crushing of concrete, may be found

$$\begin{aligned} M_{u,T} &= C_c Z \quad \text{or} \\ M_{u,T} &= T_s Z \end{aligned} \quad \text{Eq. 48}$$

If we designate ' $M_{u,exp}$ ', the capacity of the pre-cast beam determined experimentally (KEBEDE, 2009). (i.e., $M_{u,exp}$)

$$\Delta M = M_{u,exp} - M_{u,T} \quad \text{Eq. 49}$$

Where, ' ΔM ' is nothing but couple generated from compression from top reinforcement and tension from the longitudinal shear that occurs in the legs of the shear reinforcement just above the pre-cast block.

The couple generated from compression from top reinforcement and tension from the longitudinal shear that occurs in the legs of the shear reinforcement just Figure 4.7 the pre-cast concrete block.

$$\begin{aligned} \Delta M &= C_s h_s \quad \text{or} \\ \Delta M &= \tau_s h_s \end{aligned} \quad \text{Eq. 50}$$

Whichever is smaller (since failure may be initiated by either the stirrup or the top reinforcement)

$$C_s = \frac{\Delta M}{h_s} \quad \text{Eq. 51}$$

According to EBCS EN 1993 1-1:2015 section 6, the value found for ' C_s ' should be checked against; (i) Compression resistance and (ii) Bulking resistance discusses in the next section

Since the concrete is fresh, it is considered as live load, because it has a dynamic nature during pouring and unable to carry loads, precast beam is still treated as a space truss made of

steel reinforcement bars as its diagonal member. The bottom chord of the truss is subjected to tensile stress while the top chord is subjected to a compressive stress.

$$N_{t,Rd} = \frac{A f_y}{\gamma_{Mo}} \quad \text{For Tension} \quad \text{Eq. 52}$$

$$N_{b,Rd} = \frac{\chi \beta_A A f_y}{\gamma_{M1}} \quad \text{For Buckling} \quad \text{Eq. 53}$$

For main bar (longitudinal bar)

Non-dimensional slenderness $\bar{\lambda}$, may be determined from:

$$\chi = \frac{1}{\phi + \sqrt{(\phi^2 - \bar{\lambda}^2)}} \quad \text{but } \chi \leq 1 \quad \text{Eq. 54}$$

Where:

$$\phi = \frac{1}{2} (1 + \alpha(\bar{\lambda} - 0.2) + \bar{\lambda}^2)$$

α is an imperfection factor

$$\beta_A = 1$$

$$\bar{\lambda} = \frac{\lambda}{\lambda_1} \beta_A^{1/2}$$

$\lambda = \frac{L_e}{i}$, is the slenderness for the relevant buckling model

$$\lambda_1 = \pi \sqrt{\frac{E_s}{f_y}} = 93.9\varepsilon ; \quad \varepsilon = \sqrt{\frac{235}{f_y}}$$

For the sample of the cross-section is PCB-2 for S-400 and C-25 to be analyzed shown in Figure 4.7a.

$$b = 120\text{mm}$$

$$h = 80\text{mm}$$

$$d = 60\text{mm}$$

$$d'_1 = 20\text{mm}$$

$$A'_s = 113.097\text{mm}^2$$

$$A_s = 226.20\text{mm}^2$$

Solving for the unknown value of “a” in equation (45):

$$a = \frac{A_s f_y}{0.85 b f_{ck}} = 32.28\text{mm}$$

and then, using $\beta_1 = 0.8$ the depth to the neutral axis is

$$C = \frac{32.28}{0.8} = 40.35\text{mm}$$

Therefore failure is imitated by compression failure of concrete,

$$C_c = 0.8 * C * b * f_{ck} = 77.472KN$$

and from Figure 4.7

$$Z = d - 0.4C = 60 - (0.4 * 40.35) = 43.86mm$$

The moment capacity, $M_{u,T}$

$$M_{u,T} = C_c Z = 77.472KN * \frac{43.86}{1000} = 3.398 KN m$$

The capacity of the model pre-cast beam found,

$$M_{u,Exp} = \frac{(P/2)L}{3}$$

Eq. 55

$M_{u,model}$, ΔM and " C_s " are determined for each beam in Table 13

Table 13: Values of " ΔM " and " C_s " (KEBEDE, 2009)

Pre-cast Beam	Groups	Span, L (m)	P_{max} (KN)	$M_{u,exp}$ (KNm)	ΔM (KNm)	C_s (KN)	ΔM_{ave} (KNm)	$C_{s,ave}$ (KN)
PCB-1	I	3.50	6.500	7.583	4.185	23.250	4.321	20.345
PCB-2		3.50	6.600	7.700	4.302	23.900		
PCB-3		3.50	6.750	7.875	4.477	24.872		
PCB-4	II	3.00	6.750	6.750	3.352	18.622	3.752	20.844
PCB-5		3.00	7.350	7.350	3.952	21.956		
PCB-6		3.00	7.350	7.350	3.952	21.956		

For Compression resistance

$$N_{c,Rd} = \frac{A f_y}{\gamma_{Mo}}$$

Where: $A'_s = 113.097mm^2$, $f_y = 400MPa$ and $\gamma_{Mo} = 1.0$

$$N_{c,Rd} = \frac{(113.097mm^2)(400 N/mm^2)}{1.0} = 45.24KN$$

For bulking resistance, $N_{b,Rd}$

$$N_{b,Rd} = \chi \beta_A A f_y$$

Let take a bar ϕ_{12mm} , length, $l = 150mm$ (length between two nodes)

$$A'_s = \frac{\pi(12^2)}{4} = 113.097mm^2 \text{ and } f_y = 400MPa$$

$$\varepsilon = \sqrt{\frac{235}{f_y}} = \sqrt{\frac{235}{400}} = 0.77$$

$$\lambda_1 = \pi \left(\frac{E}{f_y} \right)^{0.5} = 93.9\varepsilon = 93.9 * 0.77 = 71.97$$

$$I = \frac{\pi r^4}{4} = \frac{\pi(12/2)^4}{4} = 1017.876 mm^4$$

$$i = \sqrt{\frac{I}{A}} = \sqrt{\frac{1017.876}{113.097}} = 3$$

$$\lambda = \frac{L_e}{i} = \frac{150}{3.0} = 50$$

$$\bar{\lambda} = \left(\frac{\lambda}{\lambda_1}\right) \sqrt{\beta_A} = \left(\frac{50}{71.97}\right) \sqrt{1} = 0.695$$

Buckling curve for round solid bars is 'c' (see Table 6.2, EBCS EN 1993-1-1:2015)
 Imperfection factor α for curve 'c' is 0.49

$$\chi = \frac{1}{\phi + \sqrt{(\phi^2 - \bar{\lambda}^2)}}$$

Where:

$$\phi = \frac{1}{2} (1 + \alpha(\bar{\lambda} - 0.2) + \bar{\lambda}^2) = \frac{1}{2} [1 + 0.49(0.695 - 0.2) + 0.695^2]$$

$$= 0.863$$

$$\Rightarrow \chi = \frac{1}{\phi + \sqrt{(\phi^2 - \bar{\lambda}^2)}} = \frac{1}{0.863 + \sqrt{((0.863 - (0.695)^2)}} = 0.676$$

Therefore,

$$N_{b,Rd} = \chi \beta_A A f_y = (0.676) (1) (113.097)(400) = 30.58KN$$

Check 'C_s' against:

(I) Compression resistance

$$N_{c,Rd} = A_s f_y = 45.24KN > N_{com,sd,max} = 24.872KN \quad OK$$

(II) Buckling Resistance, $N_{b,Rd}$

$$N_{b,Rd} = \chi \beta_A A f_y = 30.58KN > C_{s,max} = 20.345KN \quad OK$$

The following Table 14 depicts the summary of buckling resistance of different bar sizes.

Table 14: Buckling resistance of different sizes of bar

$f_y = 400MPa$			
Bar size (mm)	10	12	14
$A(mm^2)$	78.54	113.10	153.94
$I(mm^4)$	490.875	1017.878	1885.745
$i(mm)$	2.5	3.0	3.5
λ	60.00	50.00	42.86
ϕ	0.834	0.695	0.595
$\bar{\lambda}$	1.003	0.863	0.774
χ	0.642	0.676	0.703
$N_{b,Rd}(KN)$	20.171	30.590	43.304

Note that “ ΔM ” varies with the depth of the upper part of the pre-cast beam, span of the pre-cast beam, grade and diameters of reinforcement. The experiment was conducted for two types of pre-cast beam which varies only with their span and materials.it can be seen that experiment (Kebede M, 2009).

$$\left. \begin{aligned} \Delta M_{ave} &= 3.752 \text{ KN m} \\ C_{c,ave} &= 20.844 \text{ KN m} \\ \text{and ,} \end{aligned} \right\} \text{ For span of 3.0m}$$

$$\left. \begin{aligned} \Delta M_{ave} &= 4.321 \text{ KN m} \\ C_{c,ave} &= 20.345 \text{ KN m} \end{aligned} \right\} \text{ For span of 3.50m}$$

Note that ΔM does not vary with span length, but an experimental result makes it to vary. As can be seen from Figure 4.7, ” ΔM ” is limited by the smaller of “ C_s ” or “ τ_s ” which in turn “ τ_s ” is limited by the buckling resistance of the legs of the stirrup .The longitudinal shear “ τ_s ” which is the horizontal component of the maximum axial load that the legs of the stirrup can with stand, may be taken as the buckling resistance of the legs of the triangulated stirrups. In fact it is difficult to determine analytically the load at which buckling failure of the stirrups occur, structural software like ABAQUS can be used to analyze the truss 3D-frame by loading successively with higher loads until buckling failure of the legs of the stirrups occur. In analyzing the truss the actual uniformly distributed load on the pre-cast beam element is converted into equivalent concentrated loads at plates.

4.2.2. Prediction of the Buckling Resistance of Stirrups

The finite element analysis package such as using ABAQUS, loading the frame (by successively increasing the diameter of the part of the stirrups embedded in the pre-cast block) with successively higher loads until the mode of failure changed from failure of stirrup to failure of top reinforcement.

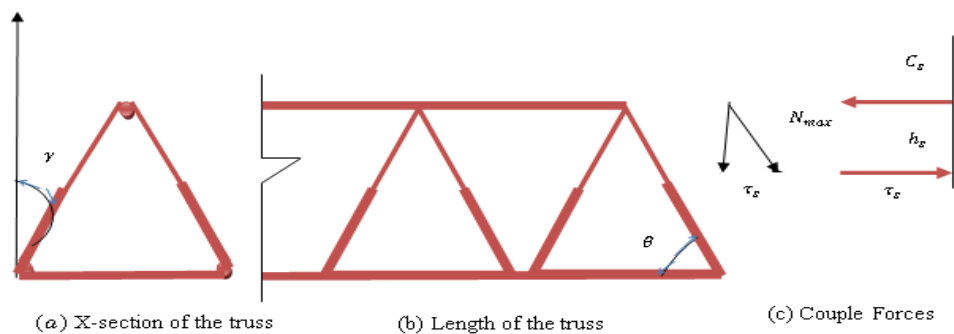


Figure 4.8: Moment capacity of upper part of the pre-cast beam

Note that the depth of the precast concrete which is effective while the beam is loaded is lower than the actual depth due to tension stiffening effect. However, in this analysis the full depth is taken for simplicity.

The maximum forces that the legs can withstand were recorded as;

$$\text{For } L = 3.0 \text{ m , } \quad N_{1,max} = 1.188 \text{ KN}$$

$$\text{For } L = 3.5 \text{ m , } \quad N_{2,max} = 1.868 \text{ KN}$$

$$\text{For } L = 4.0 \text{ m , } \quad N_{3,max} = 2.406 \text{ KN}$$

As can be seen from Figure 4.8 ,the horizontal component of the axial load contributes to the limitations for the moment capacity of the upper part of the pre-cast beam “ ΔM ” and is found to be,

$$\tau_s = 2\{N_{max} \text{ Cos } \gamma \text{ Cos } \theta\} \quad \text{Eq. 56}$$

Where:

$$\theta = \tan^{-1}\left(\frac{240}{75}\right) = 72.64^\circ, \text{ and } \gamma = \tan^{-1}\left(\frac{40}{240}\right) = 9.46^\circ$$

Since $\tau_s < C_s$ for all spans, the moment capacity of the upper part of the pre-cast beam is governed by the buckling resistance of the triangulated stirrups.

$$\Delta M = \tau_s h_s \quad \text{Where, } h_s = 180\text{mm} \quad \text{Eq. 57}$$

Equations 56 substitute in equation 57

$$\Delta M = 2\{N_{max} \text{ Cos } \gamma \text{ Cos } \theta\} h_s \quad \text{Eq 58}$$

Table 15: Moment capacity of the upper part of the precast beam

Span length ,L (m)	Maximum forces, N_{max} (KN)	τ_s (KN)	Moment Capacity , ΔM (KN m)
3.00	1.188	0.6993	0.1259
3.50	1.868	1.0996	0.1979
4.00	2.406	1.4162	0.2549

From the results found for ΔM from Table 13 (based on C_s) and above (based on τ_s), ΔM is governed by τ_s . Therefore, the capacity of the precast concrete beam can be taken as the superposition of the capacities of the precast block and the part above it.

Moment capacity of precast beam = Capacity of the Precast block

$$+ \Delta M \quad \text{Eq 59}$$

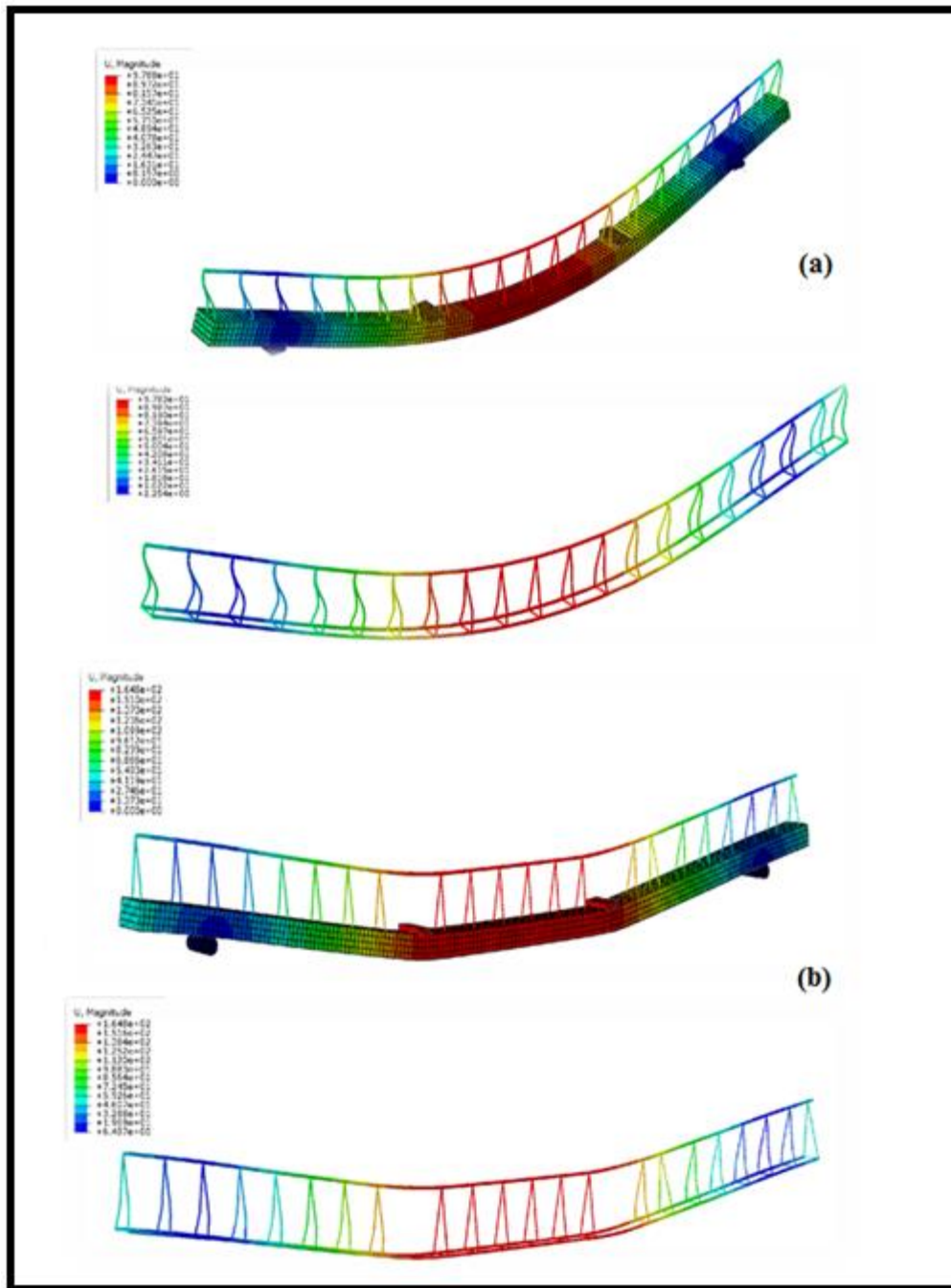


Figure 4.9: Numerical result for FEA model of Bucked stirrups: (a) For reinforcement of stirrup of 6mm diameter, (b) For reinforcement of stirrup of 8mm diameter

In this study as has been(Figure 4.9) , part of the PCB above the pre-cast block sensitive due to the low buckling resistance of the stirrups, then , increasing the stirrup amount provided greater ductile behavior given the lower yield load level compared to other precast beams in the same group showed in Figure 2.6 (b).

Figure 2.6 (b) and 4.9 is compare the buckling stirrup observed during the experimental with the failure initiated by buckling of stirrups around the supports where maximum shear and maximum moment acts simultaneously and the model of failure is shear buckling failure.

The main purpose of the Figure 4.9 was to examine the effect of the amount of the stirrups in precast beam the beam position with precast block depth 80mm on structural response. In this cause beam PCB-2 and PCB-6 of equal span length, width and depth of 80m, 120mm, and 260mm, respectively were consider but with different amount of stirrups (or shear reinforcement bar) and same spacing beam was reinforced with truss stirrups with diameter 8mm placed at 150mm spacing, while the other precast beam had the different stirrups at 150mm spacing, figure 4.9(a) and (b) respectively. The effect of stirrup reinforcement amount when it, maintained same all over the beam span figure 4.16 as show cracking pattern of the beam with stirrups spacing 150mm. the first visible crack appeared at the supported at load 4.92KN (39.40% of the ultimate load) initiating from support. As the applied load increased, other flexural and flexural- shear cracks appeared and propagated towards the top surface of the beam. However, major diagonal shear crack at the loading plate zone propagated to the top surface of beam causing buckling stirrups.

4.2.3. Load Combinations

The pre-cast beams must provide adequate strength during all stages of construction. Since the loading is different in different stages of construction, load on precast beam was calculated in different stages of construction, the following four stages of construction are considered: such as erection stage (self-weight), Block laying stage (HCB), Concrete pouring stage including Wet concrete and Construction load, and final working stage shown in Appendix A .

A structure, or part of a structure, is considered unfit for use when it exceeds a particular state, called a limit state, beyond which it infringes one of the criteria governing its performance or use (EBCS-2, 2015). „Limit states can be placed in two categories:

- a) The ultimate limit states are those associated with collapse, or with other forms of structural failure which may endanger the safety of people. States prior to structural collapse which, for simplicity, are considered in place of the collapse itself are also treated as ultimate limit states.

- b) The serviceability limit states correspond to states beyond which specified service requirements are no longer met* (EBCS-2, 2015).

There for the load combination for this specified limit states are:

$$\begin{aligned} \text{Comb 1} &= G_k + Q_k && \text{(for serviceability)} \\ \text{Comb 2} &= 1.35G_k + 1.5Q_k && \text{(for ultimate limit state)} \end{aligned}$$

4.2.4. Deflection requirement for Service Load

Normally the deformation resulting from direct axial stresses, compression or tension, are usually small, and hence no need to check. In case of flexural members, the deflection must be checked. However, because of large stiffness obtained from the cross section properties compared with those of shallow steel structures, the deflection in reinforced concrete structures do not govern the design. Nevertheless, there are cases in which designer should ensure that deflections be within limits as specified by code:

- (a) The determination of allowable deflection of precast beam: the deflections greater than about $L_e/250$ of the span are generally visible for simple and continuous beam.
- (b) For roof or floor construction supporting or attached to nonstructural elements (e.g. partitions and finishing, likely to be damaged by large deflections, that part of the deflection which occurs after the attachment of the nonstructural elements shall not exceed the value: EBCS 2-, 2015.; $\delta = L_e/350 \leq 20mm$

Among all loading stages, concrete pouring stages governs, hence deflection was checked for this loading stage.

Table 16: Deflection of Pre-cast concrete Beam at concrete pouring stage

Span (m)	3.00	3.50	4.00	4.50
Minimum Bar size (mm)	12	12	14	14
Calculated max. deflection(mm)	7.174	6.075	7.956	10.740
Maximum deflection for serviceability (mm)	8.57	10.00	11.43	12.86
Status (P/F)	P	P	P	P

Note:

- P = Pass i.e. the deflection is within the allowable limit of deflection.
- F= fail, i.e. the deflection exceeds the allowable limit of deflection

4.3. Finite Element Analysis Method

4.3.1. Numerical Simulations

This section provides detailed investigations on a developed nonlinear 3D finite-element analysis (FEA) simulation, using ABAQUS software (ABAQUS/ CAE 2014), for modeling simply-supported pre-cast concrete beam with width ($b=120\text{mm}$), depth ($h=80\text{mm}$), different span length, stirrups (Table 3), identical to that tested experimentally. The FEA model was validated using the experimental findings in terms of load-carrying capacity, buckling of stirrups, failure mode, and load–deflection response at mid span pre-cast beam. Then, the model was used to conduct a parametric analysis.

4.3.1.1. Model Set-up

A nonlinear 3D FEA model was developed considering three main elements, namely: Pre-cast concrete beam composite material, reinforced steel bars and rigid plates. The pre-cast concrete beam was modelled as a solid continuum, while steel bars were modelled using wire elements. The model utilized the 3D and eight-node linear brick solid elements with reduced integration, namely: C3D8R to simulate pre-cast concrete beam shape, in conjunction three-dimensional, two-node, truss elements, namely: B31 in ABAQUS software to simulate steel bars. Four thick plates with higher elastic stiffness were used in this modeling; two plate at the loading area and two plates at supports. Figure 4.10 shows view of the developed FEA model.

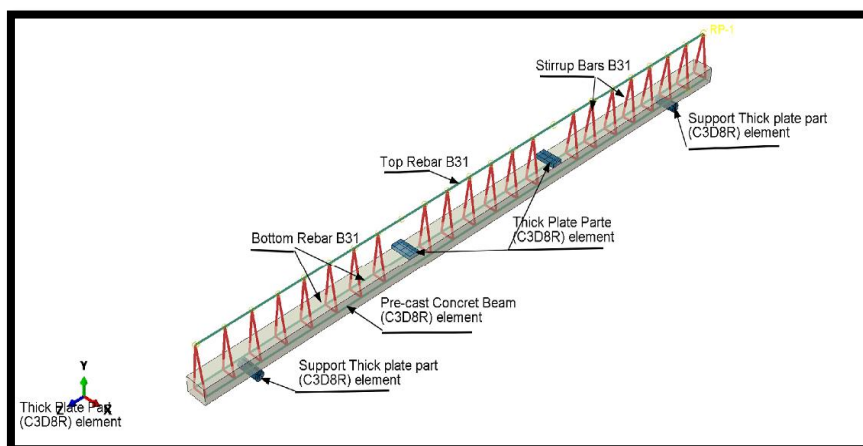


Figure 4.10: General details of the FEA model

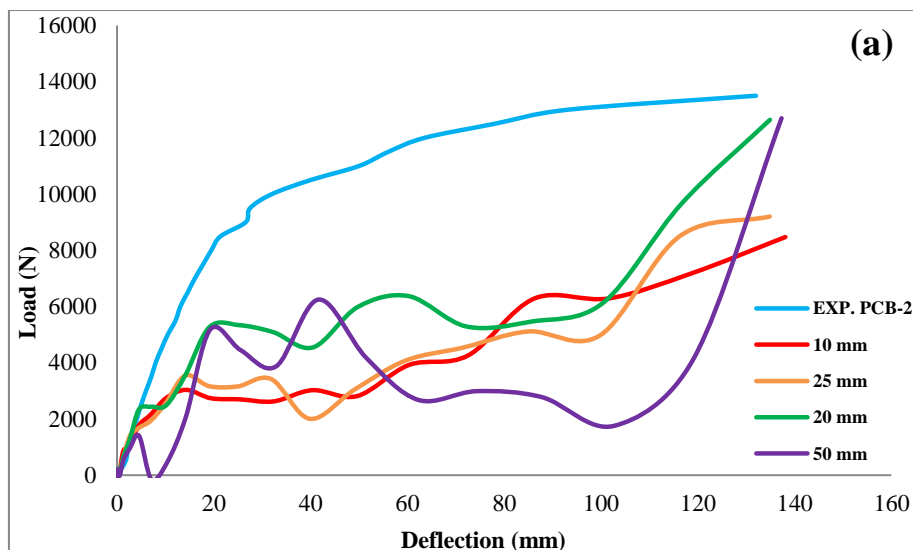
Perfect bond between reinforcing steel bars and the confined concrete was assumed to create the interaction between steel bars and surrounding concrete. This assumption was achieved

using embedded element constraint available in ABAQUS software. In such constraint, steel bars were selected to be embedded in the concrete beam as a host region.

4.3.1.2. Sensitivity of Numerical Parameters

Several attempts in the FE modelling were executed aiming to investigate the sensitivity and set-up the numerical parameters, namely: mesh density and dilation angle (ψ). These numerical parameters were examined against the experimental findings for the two control models (PCB-2 and PCB-6) in terms of load–deflection response.

The FEA models were meshed with varying element sizes, namely: 10, 20, 25 and 50 mm, leading to dividing the beam width into 12, 6, 5 and 3 elements, respectively. The load–deflection response for control models obtained experimentally and using the FEA model can be seen in Figure 4.11. It can be observed that mesh density with size of 10 and 20 mm presented a very close correlation with the experimental results prior to the ultimate stage with minor differences not exceeding about 2.6% in assessing the ultimate capacity. Due to the higher computational cost that was observed for the FEA model with 10mm mesh density, 20 mm mesh size was employed in model validation and assessment of the rest of the FEA models. The sensitivity study revealed that mesh density of 20 mm and dilation angle of 36° provided the best prediction of the structural response when compared to the experimental findings.



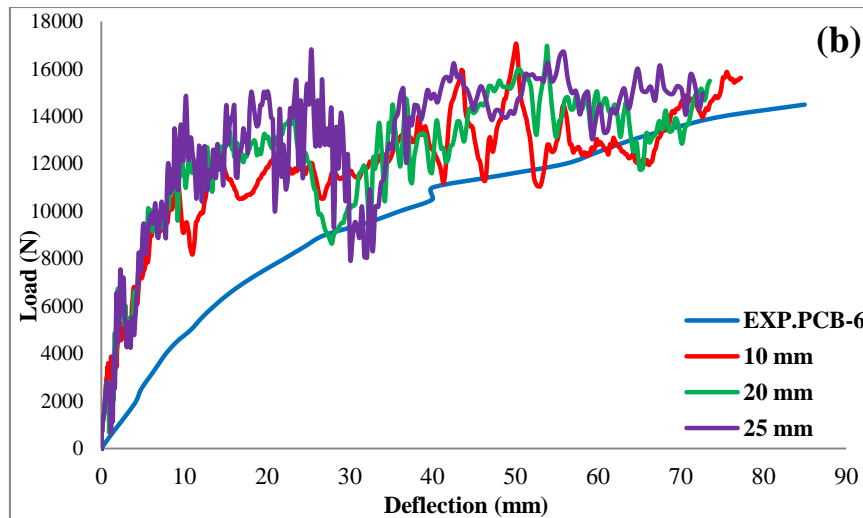


Figure 4.11: Load-deflection response observed experimentally and numerically with respect to meshing size: (a) Precast Beam, PCB-2, (b) Precast Beam PCB-6

The dilation angle mainly used in the CDP modeling is to represent the vector direction of plastic strain increment as well as the increase of stress, the applied load location and the support in the modelled beam is subjected to biaxial or tri-axial confinement, the angle value can significantly affect the numerical analysis. The angle of dilation may be selected as shown in section 4.3.1.4.

The other sensitive parameters used in the CDP model recommended elsewhere (Lubliner et al. 1989; Lee and Fenves 1998; Schickert and Winkler 1977) showed a satisfactory numerical result against those observed experimentally with negligible differences and acceptable computational cost. Such sensitive parameters were defined as follows: ratio of the second stress invariant on the tensile meridian to that on the compressive meridian (k), flow potential eccentricity (e), the ratio of biaxial to uniaxial compressive yield stresses (f_{bo}/f_{co}) and the time relaxation parameter (viscosity parameter) shown in Table 4.

4.3.1.3. Effect of tension stiffening curve

In this study tension stiffening models to get the best model that describes well the post-cracking behaviour of concrete. The models used the unified theory of concrete structure.

The tensile strength was taken as the mean bound defined in Eurocode 2, f_{ctm} . The strength criterion was adopted for all precast beams. The load deflection curve for beam (PCB-2 & PCB-6.) is shown in figure 4.11. Consequently, Hus and wang model was adopted for conducting the analysis of the test beams.

In conclusion, the approach of tension stiffening with reduced tensile concrete strength was used in the FE analyses of the test beams. Unified theory approach was used with appropriate terminal strain, ϵ_t . This terminal strain was “calibrated” based on the load deflection response.

4.3.1.4. Effect of Concrete Dilation Angle, ψ

The dilation angle of a material is a measurement of the expansion of volume occurring when the material is under shear. For a Mohr–Coulomb material like concrete, the value of dilation angle generally varies in between zero (non-associative flow rule) and the friction angle (associative flow rule). In this study, the analytical result with a value of 36° were the most closest to the experimental results.

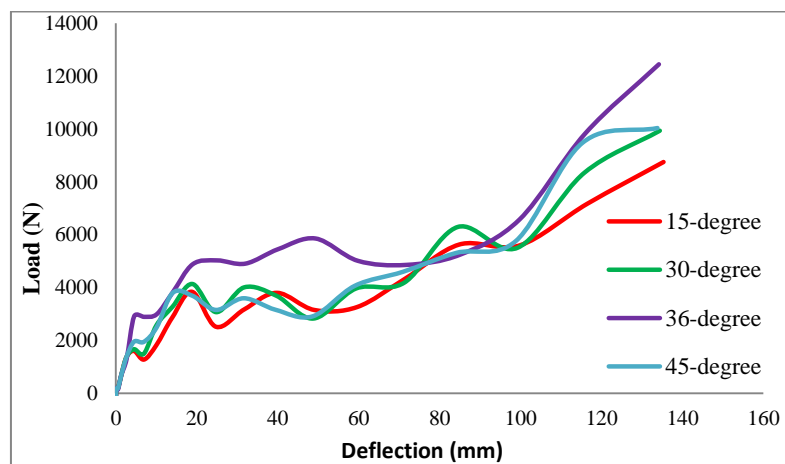


Figure 4.12: Effect of concrete dilation angle

From Figure 4.12 it can be seen, as the dilation angle increased, the deflection capacity and the failure load of the pre-cast beam was significantly increased while the required number of iterations to obtain a converged results decreased.

4.3.1.5. Effect of μ Viscosity Parameter

Material models exhibiting softening behavior and stiffness degradation often lead to severe convergence difficulties in implicit analysis programs, such as Abaqus/Standard. A common technique to overcome these convergence difficulties is the use of a visco-plastic regularization of the constitutive equations, which causes the consistent tangent stiffness of the softening material to become positive for sufficiently small time increments.

The lower value of the parameter would result in more accurate calculation and more computation time. The influence of the value of the viscosity parameter on the analytical

results is shown in Figure 4.13. As shown in this figure, with decreasing of the value of viscosity parameter, the deflection capacity and failure load increased and the required number of iterations to reach a converged solution increased. When the viscosity parameter was taken as 0.0005, the calculation results were close to the experimental results

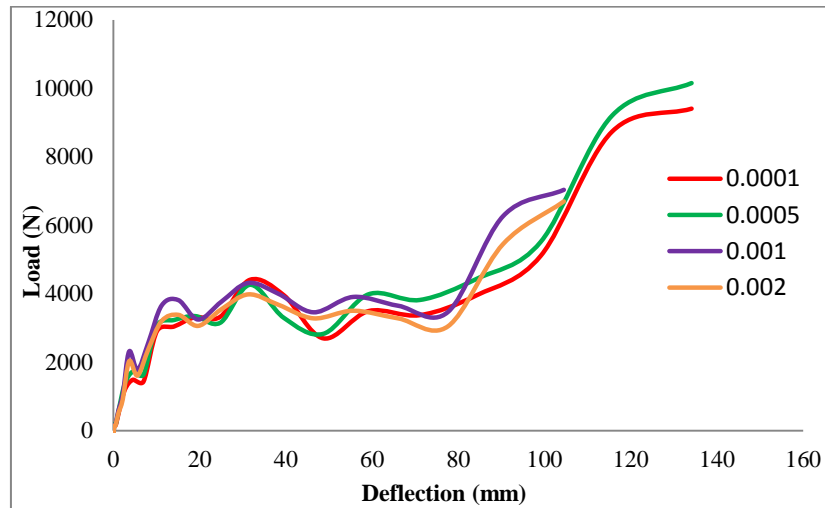


Figure 4.13: Effect of viscosity parameter, μ

4.3.2. Validation of Finite Element Model

4.3.2.1. C crack Pattern and Failure Mode

This section discusses and compares the results obtained experimentally and numerically from the static tests performed on the two controls pre-cast concrete beams are PCB-2 and PCB-6. Table 17 provides the recorded values of first visual cracking load $P_{cr,FE}$, ultimate load $P_{u,FE}$, maximum deflection at both cracking and ultimate stages; δ_{cr} and δ_u respectively.

Table 17: Comparison between FEA results and Experimental

Designation	Cracking Properties		P_y (KN)	P_u (KN)	δ_{cr} (mm)	Model of Failure
	P_{cr} (KN)	δ_{cr} (mm)				
EXP. PCB-2	6.60	16.090	12.500	13.500	132.00	F
EXP. PCB-6	7.500	19.600	13.277	14.500	85.00	F
FEA PCB-2	5.184	19.269	9.672	12.643	134.890	F
FEA PCB-6	8.754	11.258	11.561	14.973	72.683	F

P_{cr} , load at which first crack occurred; δ_{cr} , deflection recorded at first crack; P_y , load at which first yield occurred; P_u , ultimate load; δ_u , deflection recorded at ultimate load; , first yield load recorded at flexural bar; H, first yield load recorded at horizontal bar; MS, mid-length of strut connect between , edge of loading plate and support; F, flexural failure.

Figures 4.14 and 4.15 provide the tensile and compressive cracking visualization for the numerical models PCB-2 and PCB-6, respectively. It should be noted that cracking pattern view is available in ABAQUS software through maximum plastic strain. Cracking can be considered in CDP models when maximum principle stresses achieve the positive sign. Also, the crack propagation is assumed to be perpendicular to maximum principle plastic strain.

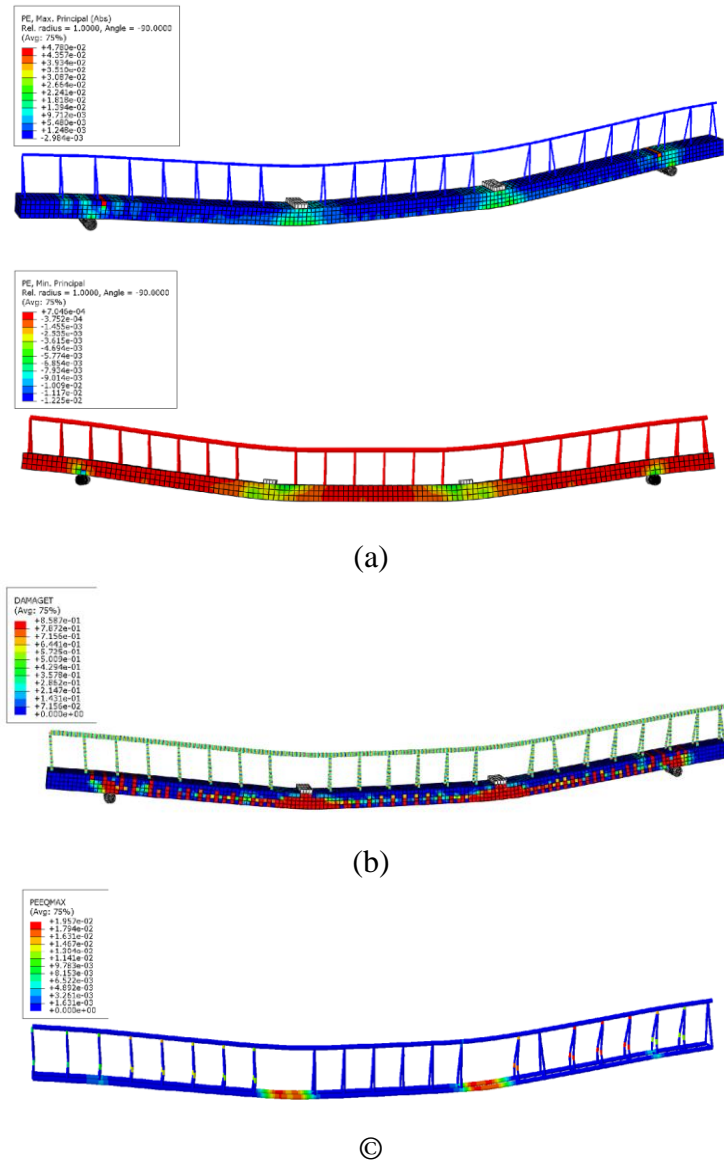


Figure 4.14: Numerical result for FEA modeling of beam PCB-2; (a) contour lines of compression stresses along precast beam span; (b) tensile damage of along precast beam span; (c) contour line steel stress distribution.

When maximum principle stresses achieve the positive sign. Also, the crack propagation is assumed to be perpendicular to maximum principle plastic strain. Similar to experimental crack pattern of beam PCB-2 shown in Figure 2.6, numerical simulation shown in Figure 4.14 shows tensile stresses causing the first cracking at the bottom beam-surface close to

loading section at a load $P_{cr,FE}$ of 4.92 KN. Also, model PCB-2 presented very critical stresses leading to first crack extending from the bottom reinforcement bars.

At higher increments, significant compressive strut connecting between loading location and supporting plates for beam PCB-2 was captured numerically as shown in Fig.4.14b and experimentally in Figure 2.6(a). Significant tensile cracking stresses were observed initiating from bottom of precast beam PCB-2 expanding upward towards the loading plate zone as shown in the FEA model views in Figure 4.14(a) and experimentally in Figure 2.6(a) through appearance of flexural cracks. In addition, very few flexural cracks appeared at the bottom surface at section close to loading plate and propagated towards the top of the beam with increase in applied loading.

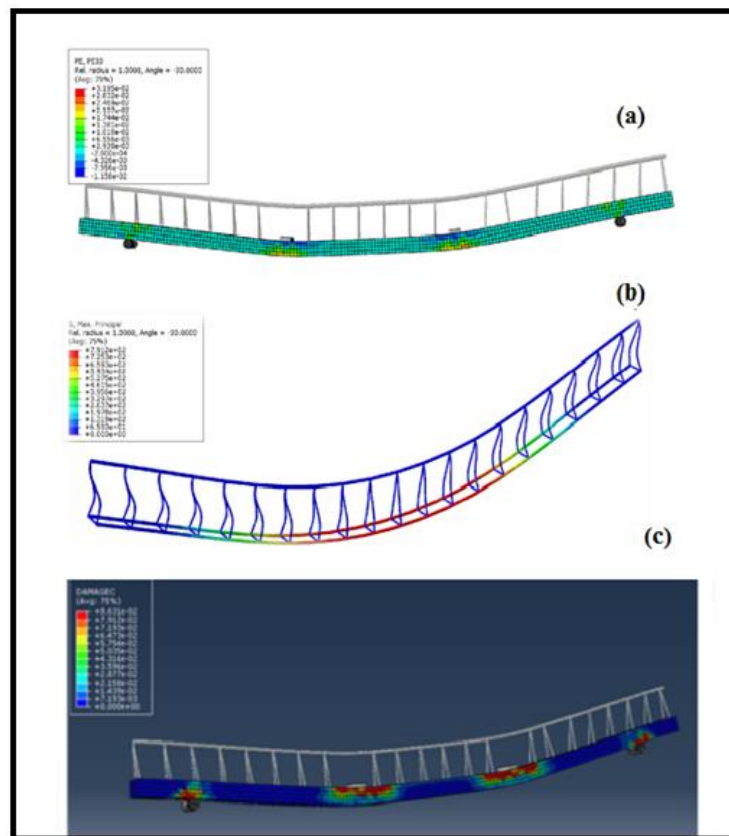


Figure 4.15: Numerical results for FEA modeling of beam PCB-4: (a) contour lines of tensile stresses along beam span; (b) contour lines of tensile stresses at bottom reinforcement bar; (c) compression damage of along precast beam span.

Just before failure of beam PCB-2, the major strut formed at shear zone grew presenting higher compressive stresses at its two ends (i.e. close to loading and supporting plates) as shown in Figure 4.14 (a). However, such compressive stresses were slightly excessive close to loading plate leading to failure at $P_{u,FE}$ of 12.643KN (about 93.65% of $P_{u,EXP}$ as depicted

in Table 17) with similar failure mode observed experimentally as shown in Figure 2.6(a). For FEA model PCB-2, the major tensile cracking stresses formed at bottom surface propagated upward towards top surface as shown in Figure 4.14(c), and then tensile stresses peaked at top surface in contact with the loading plate as shown in Figure 4.15(a), leading to failure at an ultimate load $P_{u,FE}$ of 14.973KN (about 96.74 % greater than $P_{u,EXP}$ as shown in Table 17). Such numerical compressive failure was almost similar to the brittle concrete crushing observed experimentally at the edge of loading plate shown in Figure 2.6(a) reflecting the occurrence of compressive action.

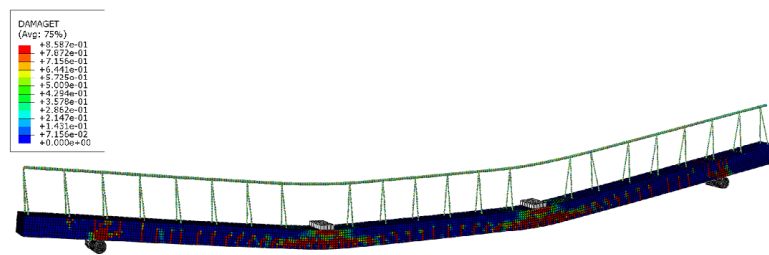


Figure 4.16: Flexural cracking

Figure 2.6(a) and 4.16 is compare the damage observed during the experiments with the damage predicted in the simulation. In the experiments, testing was terminated when brittle failure (concrete crushing) occurred. Figure 2.6 shown that at the peak load, concrete crushing occurred at top of the load applied parts, and flexural cracking (maximum principal plastic strain) was observed at the bottom surface of the pre-cast beam.

4.3.2.2. Load-Deflection Response at Mid span

The finite element analysis capture load carrying capacity, mid-span deflection and failure model. The dependent variables that are used to validate the finite element analysis with experimental test are tabulated as follows.

Table 18: Comparison FEA and Experimental result

Experimental test	Dependent variable	FE model	Experimental result	Difference	Percentage difference
Validation one PCB-2	Ultimate load (KN)	12.643	13.500	0.857	6.348
	Mid-span deflection (mm)	134.890	132.00	2.890	2.189
Validation two PCB-6	Ultimate load (KN)	14.973	14.500	0.473	3.262
	Mid-span deflection (mm)	72.683	85.00	12.317	14.491

The six no's of precast beam specimens tested under static loading and six no's of precast beam specimens tested under static loading were analyzed using the ABAQUS. The results pertaining to the objectives of the study are presented and discussed in this section. The finite element analysis results of the precast beams and specimens are presented in Table 3. The six no's of precast beam specimens were tested under static loading. The test results were analyzed by using ABAQUS nonlinear finite element analysis. The test results obtained experimentally and those obtained through nonlinear finite element analysis were compared and discussed. The precast beam PCB-2 exhibit an experiment ultimate load of 13.50kN, the corresponding deflection obtained through experiment (132mm) and FEA using ABAQUS ultimate load of 12.643KN, the corresponding deflection obtained through FEA (134.890mm) varied by 6.348% and 2.189% respectively. The beam PCB-6 exhibit an experiment ultimate load of 14.50kN, the corresponding deflection obtained through experiment (85mm) and FEA using ABAQUS ultimate load of 14.973KN , the corresponding deflection obtained through FEA (72.683mm) varied by 3.262% and 14.491% respectively. Figure 4.17 and 4.18 explains Load Vs Deflection behavior of ABAQUS Vs. Experimental values

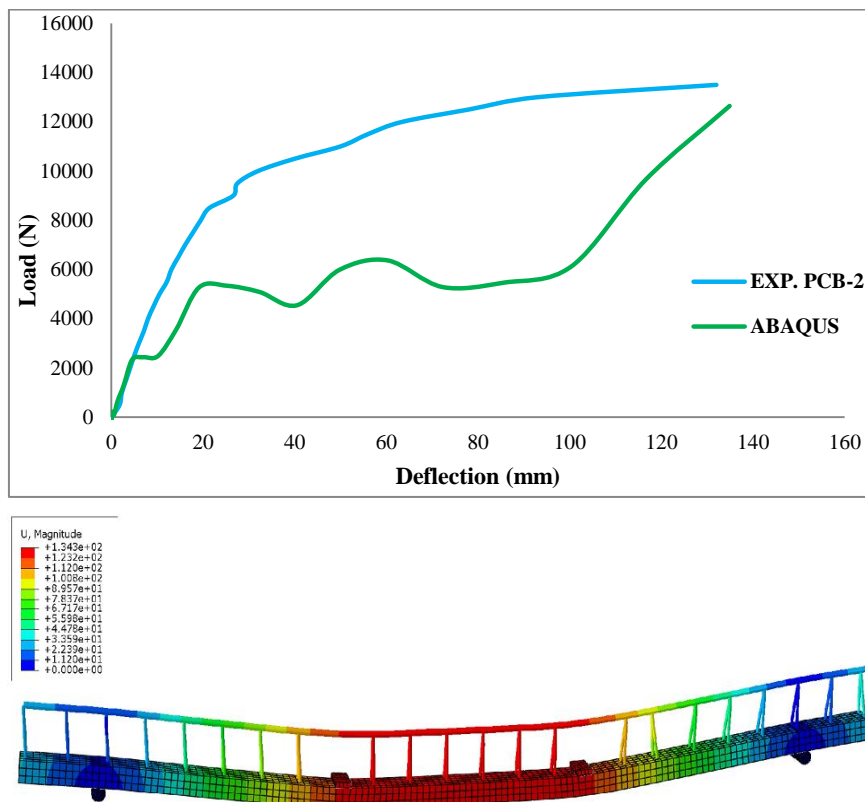


Figure 4.17: Load – Deflection response observed experimentally and numerically with respect to meshing size for Pre-cast beam, PCB-2

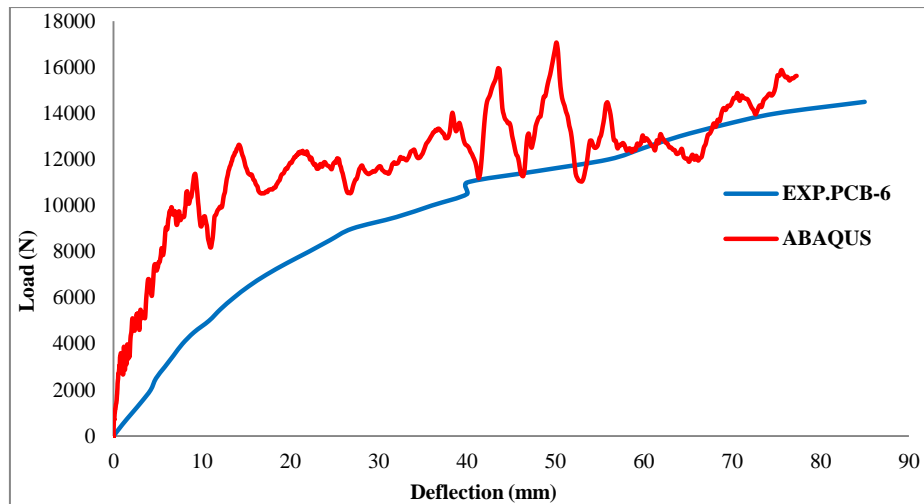


Figure 4.18: Load – Deflection response observed experimentally and numerically with respect to meshing size for Pre-cast beam, PCB-4

This section discusses and compares the results obtained experimentally and numerically from the static tests performed on the two control pre-cast beams PCB-2 and PCB-6. The Experimental and numerical load–deflection relationship measured at the mid-span of the pre-caste beam of the PCB-2 and PCB-6 are depicted in Figure 4.17 and 4.18. Other than the earlier discussion regarding cracking load and mode of failure, one may observe that both numerical and experimental results showed similar elastic behavior ending at almost the same yield load with a difference of about 6.35 % as shown in Table 18. Also, the load–deflection response for beam PCB-2 shown in Figure 4.17 shows good agreement between the FEA Modelling and the experimental findings.

4.3.2.3. Effect of Compressive Strength

The current numerical model was utilized to show the effect of compressive strength on the behavior of precast beam. The concrete compressive cylinder strength was varied in the range of 20, 25, and 30 MPa. The other parameters are kept the same for precast beam PCB-2. The influence of (f_{ck}) on the performance of precast beam is shown in figure 19. The maximum load of PCB-2 beams increases with the increase of the concrete compressive strength. The maximum load, of the PCB-2 beam decreases from 9.763kN for $f_{ck} = 20\text{MPa}$ to 11.830KN for $f_{ck} = 30\text{MPa}$. The increasing of failure load is almost slightly diverging from compressive strength. The load deflection behavior is illustrated in Figure 4.19 for altered estimations of concrete compressive strength.

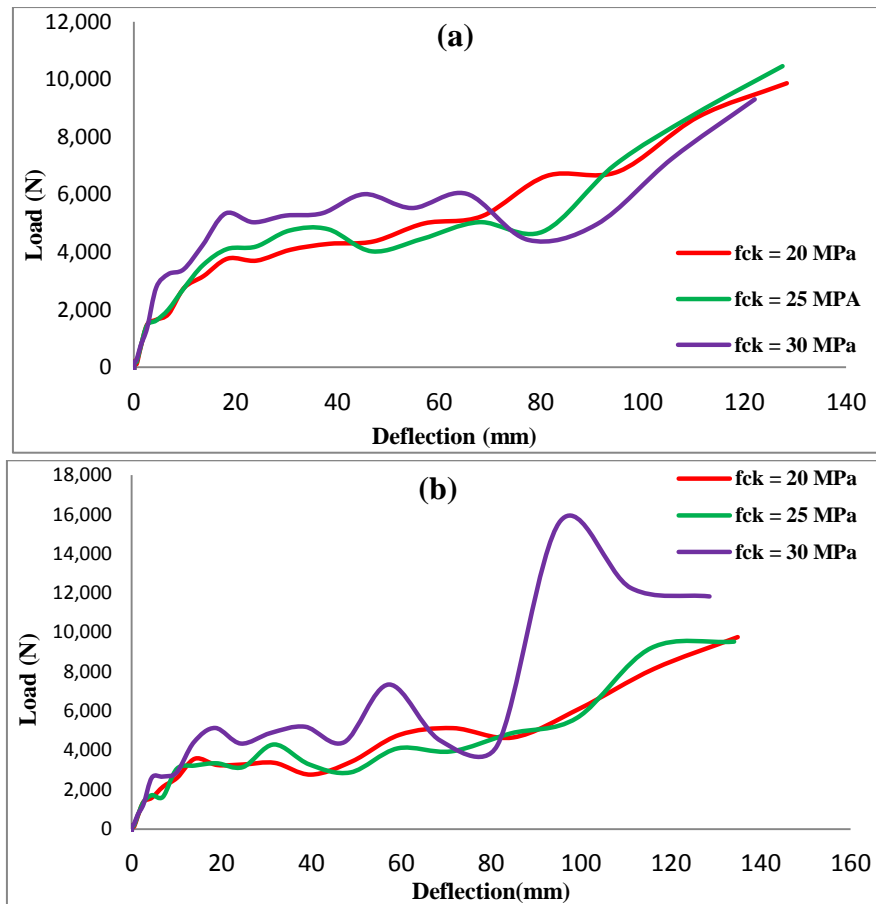


Figure 4.19: load-deflection behavior for different value of f_{ck} (a) PCB-2, (b).PCB-6

CHAPTER FIVE

CONCLUSION AND RECOMMENDATIONS

1.1. CONCLUSION

- 1) In this study, the model taken in to consideration the nonlinear properties for concrete and steel used unified theory of concrete structure. The numerical results proposed from the FE model then compared with the experiment data to have a good verification. The result showed that the predicated loads and deflections of the precast concrete beam by the present FE models were found to be agrees well with the experimental data.
- 2) In addition, some parameters such as tension stiffening effect, mesh sensitivity effect have been studied
- 3) In this study, Softened truss model was developed for the nonlinear analysis of concrete membrane elements. This model involves three equilibrium equation, three compatibility equation and four equations for constitutive laws of concrete and steel. Based on the unified theory reinforced concrete structure, smeared stress-strain relationships have been determined for concrete in compression, concrete in tension, and steel reinforcement embedded in concrete.
- 4) In modified version of the constitutive laws, the smeared tensile stress-strain curve of concrete is used in conjunction with the elastic-perfectly-plastic stress-strain relationship of bare mild steel bars. This combination of constitutive law will take care of tension stiffening effect on deformations, but will also result in a significant overestimation of yield strength. If the concrete in tension is neglected, however, as in the simplified version of constitutive laws, the deformation at service load will be significantly overestimated.
- 5) Since the maximum deflection of bare bar is much greater than stiffened bar both by self-weight and design load, hence the contribution of concrete is significant for deflection.
- 6) The maximum deflection of the beam without role of concrete is greater than the allowable deflection of pre-cast beam, and the maximum deflection of the pre-cast beam with the role of concrete is less than allowable deflection. Therefore, the beam is satisfies serviceability requirement for deflection of pre-cast beam.
- 7) Based on the validation of finite element model against experimental results and parametric study with varied values of dilation angle, viscosity parameter, and static load, following conclusions can be made:

- The Finite element analysis model in ABAQUS can predict the concrete crushing failure mode in precast concrete beam. The pre-cast beam PCB-2 exhibit an experiment failure load of 13.5KN, the corresponding deflection obtained through experiment (132mm) and FEA using ABAQUS failure load of 12.643KN , the corresponding deflection obtained through FEA (134.89mm). The numerical error of the failure loads and mid-span deflection was within 6.635% and 2.189%, respectively.
 - The pre-cast beam PCB-6 an experiment failure load of 14.50KN, the corresponding deflection obtained through experiment (85mm) and FEA using ABAQUS failure load of 14.973KN, the corresponding deflection obtained through FEA (72.683mm). The numerical error of the failure loads and mid-span deflection was within 3.26 % and 14.49%, respectively.
- 8) This study investigated that how different parameter like concrete strength, steel yield strength, reinforcement bars; affect the static load of pre-cast beam. From simulation conducted in this study the following conclusion is made.
- From the validations it has been observed that is imitated by buckling of stirrups around the supports where maximum shear and maximum moment acts simultaneously and the mode of failure is shear buckling failure.
 - As has been the validation of bucking resistance, part of the precast concrete beam above the pre-cast block is sensitive due to the low buckling resistance of the stirrups. Therefore, the moment capacity of the pre-cast beam is highly influenced by the contribution of part of the PCB above the pre-cast block for the critical loading stage.

1.2. RECOMMENDATIONS

The following recommendations are made for future researchers to investigate further by considering:

- 1) Since failure occurs around the supports where maximum shear and maximum moment simultaneously acts ,the capacity of the precast beam can be improved by decreasing the space between the nodes of the stirrups around the support, and decreasing the height of the part of the precast above the precast block
- 2) In this study only precast concrete beam was considered. Therefore, it is recommended for future investigators experimental to consider other span length, material property of concrete and reinforcement bars.

REFERENCE

- 1) **A. Alfarach F.Lopez-Almansa, S.Oller** New Methodology for calculating damage variables evolution in plastic Damage Model for RC Structures. Barcelona , Spain :, 2016. - Vol. 132.
- 2) **ABAQUS** ABAQUS Analysis user's Manual . Boston , U.S.A, 2014.
- 3) **Barkanov E.** Introduction to the Finite Element Method : Riga Technical university, 2001.
- 4) **Budarin A. Alekhin , Avdonina L.** Numerical modelling of the reinforced concrete beam shear failure. International Conference on Construction, Architecture , Russia : IOP, 2019. - Vol. 687.
- 5) **CHIRUTA GEORGE.** Finite-element modelling of reinforced concrete: Aalborg University, 2014.
- 6) **Committe PCI Industry Handbook** .PCI design hand book Precast and Prestressed Concrete. Chicago , 1999. ISBN 0-937040-60-6.
- 7) **Construction Ministry of Urban Development and Design of Concrete Structures** ,EBCS-2 EN 1992-1-1:2015 . Addis Ababa,Ethiopa : Ministry of Construction, 2015.
- 8) **Dina Mohammed, Fathi Ors ,Hussein Osama Okail, & Amr Hussien Zaher** .Modeling of Shear deficient beams by the mixed smeared/diserete cracking approach. Egypt : Elsevier, 2014. - Vol. 12.
- 9) **Euro-code 2**, Design of concrete structures. Part 1-1, General rules and rules for building . Brussels, 2004. - Vol. 2.
- 10) **Hibbitt Karlsson and Sorensen ,Inc.2014** .ABAQUSE/ CAE User;s Manual. Boston : U.S.A, 2014. - MA 02111-1307.
- 11) **Kebede M.** Analysis, Design and Cost Effectiveness of Precast Beam-Slab System. Addis Ababa : M.se. thesis, 2009.
- 12) **Li-Jian** Based on ABAQUS of concrete structure nonlinear finite element analysis: Switzerland , 2013. ISSN : Vols. 756-759, pp 186-189. - 1662-8985.
- 13) **LV Xi-lin., JIN Guo-fang &WU Xiao-han.** Reinforced Concrete Structure Nonlinear Theory and Applications. - Shanghai : Tongji University Press, 1997.
- 14) **MH GTZ** .Technical Manual for Low cost Housing . - Addis Ababa : , 2005.
- 15) **Ramaswamy K. J. Bathe and S.** On Three-Dimensional nonlinear analysis of concrete Structures : Nucl. Engng Des. , 1989. - Vols. 52, 385-409.
- 16) **Sihua Deng Ze Qie & Li Wang** . Nonlinear Analysis of Reinforced Concrete Beam Bending Failure Experimentation Based on ABAQU. - Beijing China : Atlantis Press, 2015.
- 17) **Thomas T.C Hsu.** Unified Theory of Concrete structures: John Wiley and sons,Ltd, 2010. - Vol. 1.

- 18) **Toshimi Chen, Shaohua and Kabeyasawa.** AVERAGE STRESS-STRAIN RELATIONSHIP OF STEEL BARS EMBEDDED IN CONCRETE: 13th World Conference on Earthquake Engineering. - Canada : Vancouver, B.C., Canada , 2004. Vol. 3290 .
- 19) **Wang T. C. and Hsu T.** Nonlinear finite element analysis of concrete structure using new constitutive model computers and structure.- 2011.- 32: Vol. 79.
- 20) **ZHUANGZhuo ZHANG Fan, CEN Song.** ABAQUSE Nonlinear Finite Element Analysis and Examples .- Beijing : Beijing Science Press, 2005.Vols. 123-139.

APPENDIXES

APPENDIXA -A: LOADING

A-1 Load Calculation

Since the loading is different in different stages of construction, load on precast beam was calculated in different stages of construction, the following four stages of construction are considered: such as erection stage (self-weight), Block laying stage (HCB), Concrete pouring stage including Wet concrete and Construction load, and final working stage.

In this study, PCB-2 was used as sample Precast beam:

Geometrical Property of precast Beam :

- ✓ Width, $b = 120mm$
- ✓ Depth of precast concrete beam , $h = 80mm$
- ✓ Depth of slab, $D = 280mm$
- ✓ Effective depth, $d = 280mm - 20mm - 20mm = 240mm$
- ✓ Center to center distance between ribs = $600mm=0.60m$

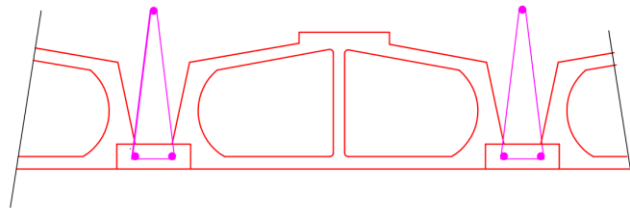


Figure A-1.1:Pre-cast beam and HCB arrangement before top slab casing /at initial condition

A-1.1. Erection Stage

Erection stage of construction only self-weight of the precast beam is considered as a dead load and has no live load:

$$\text{Self-Weight of precast beam, } G_k = (0.12m \times 0.08m) \times 25 \text{ KN/m}^3 = 0.24 \text{ KN/m}$$

Since the model is truss, only a concentrated load is acted on the joints, hence the calculated uniformly distributed load has to be changed to concentrated (or point) load

$$\text{Concentrated load, } g_k = 0.24 \text{ KN/m} \times 0.15m = 0.036 \text{ KN}$$

A-1.2. Block Laying Stage

Block laying stage on self-weight of pre-cast beam and slab block is considered as a dead load and self-weight of the block layer as a live load:

Dead Load:

- ✓ Weight of precast beam, $G_k = (0.12m \times 0.08m) * 25 \text{ KN/m}^3 = 0.24 \text{ KN/m}$
- ✓ Weight of HCB, $G_{k,HCB} = A_{HCB} \times \gamma_{HCB} = 0.0511 \times 17 \text{ KN/m}^3 = 0.8687 \text{ KN/m}$
- ✓ Total dead load , $G_k = 0.24 \text{ KN/m} + 0.8687 \text{ KN/m} = 1.1087 \text{ KN/m}$

- ✓ Concentrated point load, $g_k = 1.1087 \text{ KN/m} \times 0.15\text{m} = 0.166305 \text{ KN}$

Live load: Construction load:

- ✓ Load during erection (assumption) depending on structure = $1 \text{ KN/m}^3 \times 0.6\text{m} = 0.6 \text{ KN/m}$

$$Q_k = 0.60 \text{ KN/m}$$

- ✓ Concentrated Point load, $q_k = 0.60 \text{ KN/m} * 0.15 = 0.090\text{KN}$

Design load,, P_d :

$$P_d = 1.35G_k + 1.50Q_k = 2.39675 \text{ KN/m}$$

A-1.3. Concrete Pouring Stage

Concrete pouring stage since the concrete is wet/ fresh it cannot supports its self-weight and other loads but during poring and compacting, there will be a vibration, therefore, weight of fresh concrete is considered as a live load.

Dead load, G_k :

- ✓ Weight of precast beam, $G_k = (0.12\text{m} \times 0.08\text{m}) * 25 \text{ KN/m}^3 = 0.24 \text{ KN/m}$
- ✓ Weight of HCB, $G_{k,HCB} = A_{HCB} \times \gamma_{HCB} = 0.0511 \times 17 \text{ KN/m}^3 = 0.8687 \text{ KN/m}$
- ✓ Total dead load , $G_k = 0.24 \text{ KN/m} + 0.8687 \text{ KN/m} = 1.1087 \text{ KN/m}$
- ✓ Concentrated point load, $g_k = 1.1087 \text{ KN/m} \times 0.15\text{m} = 0.166305\text{KN}$

Live load, Q_k :

- ✓ Load during erection (assumption) = $0.5 \text{ KN/m}^3 \times 0.6\text{m} = 0.30 \text{ KN/m}$
- ✓ Concentrated load = $0.30 \text{ KN/m} * 0.15 = 0.045\text{KN}$
- ✓ Wet/Weight of fresh concrete = $(0.6 * 0.28) - (0.105 + (0.12 * 0.08)) * 25 = 1.335 \text{ KN/m}$
- ✓ Total Live load, $Q_k = 1.635 \text{ KN/m}$
- ✓ Concentrated point load, on the joints other than the middle four joints

$$q_{k,f} = 0.24525\text{KN}$$

But on the middle four joints the self-weight of the laborer is considered in addition to the Weight of fresh concrete, hence

$$q_k = 0.29025 \text{ KN}$$

Design load, P_d :

$$P_d = 1.35G_k + 1.50Q_k = 3.9492 \text{ KN/m}$$

A-1.4. Final Working Stage

Final working stage of construction since the concrete gets its hardness, the whole system no more considered as space truss rather it is treated as a normal beam structure.

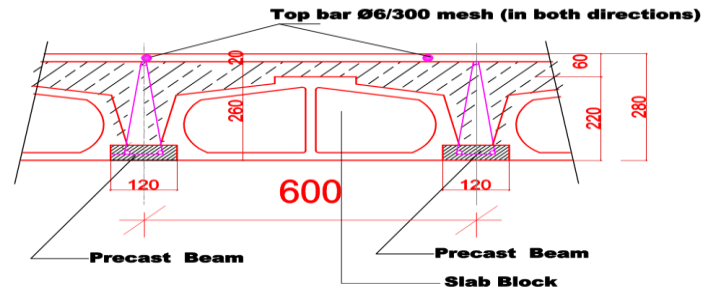


Figure A-1.2: Section of precast beam and slab at final condition

Dead Load, G_k :

- ✓ Weight of Pre-cast Beam = $(0.12m \times 0.08m) \times 25 \text{ KN/m}^3 = 0.24 \text{ KN/m}$
- ✓ Weight of HCB (Hollow Concrete Block) = $A_{HCB} \times \gamma_{HCB} = 0.8687 \text{ KN/m}$
- ✓ Weight of cast in-situ concrete = $0.0512 \times 25 \text{ KN/m}^3 = 1.280 \text{ KN/m}$
- ✓ Cement screed = $t * b * \gamma_c = 0.05m \times 0.60m \times 23 \text{ KN/m}^3 = 0.690 \text{ KN/m}$
- ✓ Ceiling plaster = $t * b * \gamma_c = 0.02m \times 0.60m \times 23 \text{ KN/m}^3 = 0.276 \text{ KN/m}$
- ✓ Partition wall, $1.0 \text{ KN/m}^2 = 1.0 \text{ KN/m}^2 \times 0.60m = 0.60 \text{ KN/m}$
- ✓ Total Dead load, $G_k = 0.24 \text{ KN/m} + 0.8687 + 1.28 \text{ KN/m} + 0.69 \text{ KN/m} + 0.276 + 0.6$
 $= 3.9547 \text{ KN/m}$

Live load (Q_k):

- ✓ Residential area, 2.0 KN/m^2 , $Q_k = 2.0 \text{ KN/m}^2 \times 0.625m = 1.25 \text{ KN/m}$

Design load, (P_d):

$$P_d = 1.35G_k + 1.50Q_k = 7.13885 \text{ KN/m}$$

$$\text{Concentrated point load, } P_c = 1.070827 \text{ KN}$$

Appendix A -2: Deflection of the final working Stage

Table A-2.1: Compressive and tensile force on the horizontal member of the truss model of precast beam

Span (m)	3.00	3.50	4.00	4.50
Bar Size (mm)	12	12	14	14
Tensile force (KN)	11.78	16.71	21.94	41.36
Tensile resistance (KN)	45.24	45.24	61.58	61.58
Compressive force (KN)	11.78	16.71	21.94	41.36
Compressive resistance (KN)	30.59	30.59	43.31	43.31

Table A-2.2: Compressive and tensile force on the diagonal member of the truss model of precast beam

Material	$f_y = 400MPa$				
Span(m)	3.00	3.50	4.00	4.50	5.00
Tensile force (KN)	7.638	6.546	5.728	5.092	4.583
Tensile resistance (KN)	10.310	10.310	10.310	10.310	10.310
Compressive force (KN)	2.310	3.520	6.081	8.260	6.940
Compressive resistance (KN)	2.436	2.436	2.436	2.436	2.436

As we see from the summarized Table A-2.2 that except for a span length of 3.00m, the compressive force exceeds the compressive resistance of stirrups/ diagonal member of the space truss model, hence if the size of reinforcement is changed to diameter 8 mm bar for the spans of 3.5m and 4.00m. The resulting compressive resistance will be 5.89kN; beyond a span of 4.0m a central supporting prop must be provided.

Table A-2.3: Deflection at final working stage

Span (m)	3.00	3.50	4.00	4.50
M_k (KN m)	5.855	7.970	10.409	13.174
K_m	27.00	31.35	35.82	40.30
k_x	0.110	0.152	0.174	0.209
k_z	0.960	0.944	0.926	0.917
x (mm)	63.03	63.03	71.87	71.87
z (mm)	196.97	196.97	188.13	188.13
δ_i (mm)	0.4197	0.5713	0.746	0.944
δ_{ii} (mm)	1.528	4.1304	6.045	13.668
δ_{Max} (mm)	3.127	5.7943	7.960	14.268
$\frac{L_e}{350}$	8.570	10.00	11.43	12.86

Table A-2.4: Deflection at the final working stage

Span (m)	3.00	3.50	4.00	4.50
M_k (KN m)	5.855	7.970	10.409	13.174
K_m	25.00	31.35	35.82	40.30
k_x	0.110	0.152	0.174	0.209
k_z	0.960	0.944	0.926	0.917
x (mm)	63.03	63.03	71.87	71.87
z (mm)	196.97	196.97	188.13	188.13
δ_i (mm)	0.4860	0.662	0.864	1.1056
δ_{ii} (mm)	0.9787	3.382	7.645	11.219
δ_{Max} (mm)	3.127	5.7943	7.960	14.268
$\frac{L_e}{350}$	8.570	10.00	11.43	12.86

We can see from the Table 17 that deflection limits is not satisfied for a span beyond 4.50m hence a beam of this model can only be has less than 4.5 m.